Best Practices for Solar Irradiance Measurements with Rotating Shadowband Irradiometers

A report of IEA SHC Task 46, Solar Resource Assessment and Forecasting

August 18th, 2015

S. Wilbert, N. Geuder, M. Schwandt, B. Kraas, W. Jessen, R. Meyer, B. Nouri

SOLAR HEATING & COOLING PROGRAMME
INTERNATIONAL ENERGY AGENCY

Prepared within IEA Task 46, Subtask B1 and INS project 1268

Contents

1. Introduction

Large-scale solar plant projects require diligent solar resource assessments. For concentrating solar technologies the focus of the resource assessment lies on direct beam irradiation. Unfortunately, high accuracy irradiance data are scarcely available in regions which are attractive for solar energy applications. Satellite data can only be used in combination with ground data to estimate inter-annual variability and long-term mean values. Hence, new ground measurements have to be collected for solar plant projects.

Ground measurement data usually show significantly higher accuracies than satellite derived irradiance data, when general guidelines regarding site selection and preparation, instrument selection and maintenance and data quality monitoring are respected. These best practices for Rotating Shadowband Irradiometers (RSIs) are presented in this document.

Appropriate irradiance sensors for ground measurements must be selected in consideration of general surrounding conditions for equipment and maintenance to gain and maintain the necessary accuracy over the entire operation period. Thermopile instruments like pyrheliometers as specified in ISO standard 9060 [ISO9060 1990] are severely affected by soiling [Pape2009] and also require expensive and maintenance-intensive support devices such as solar trackers and power supply. Thus, the uncertainty of resource assessment with pyrheliometers depends heavily on the maintenance personnel and cannot be determined accurately in many cases. Due to their low soiling susceptibility, low power demand, and comparatively lower cost, Rotating Shadowband Irradiometers (RSI) show significant advantages over the thermopile sensors when operated under the measurement conditions of remote weather stations. RSIs are also known as RSP (Rotating Shadowband Pyranometers) or RSR™ (Rotating Shadowband Radiometers). Here we use the notation RSI to refer to either instrument measuring irradiance by use of a rotating shadowband following the decision of the international expert group in IEA Solar Heating and Cooling Task 46, subtask B. The initially lower accuracy of RSIs, which can yield deviations of 5 to 10 % and more, is notably improved with proper calibration of the sensors and corrections of the systematic deviations of its response. Main causes of the systematic deviations are the limited spectral sensitivity and temperature dependence of the Si-photodiode commonly used in most RSIs.

Besides the systematic deviations of the sensor response, a significant contribution to the measurement inaccuracy originates from the sensor calibration at the manufacturer, where no corrections are applied. For proper calibration however, the proposed corrections need yet to be considered in the calibration procedure. While well documented standards exist for the calibration of pyrheliometers and pyranometers ([ISO9059 1990], [ISO9846 1993], [ISO9847, 1992]) they cannot be applied to RSIs and no corresponding standards exist for RSIs

This document contains RSI specific best practices for the following tasks:

- Requirements on the selection of a location for a measurement station
- Installation, operation and maintenance of a measurement station, including the case of remote sites
- Documentation and quality control of the measurements
- Correction of systematic errors & instrument calibration: procedure and frequency

Also the performance and accuracy of RSIs are described.

2. General description of continuously rotating RSIs

A continuously rotating RSI itself consists of a horizontally mounted LI-COR pyranometer in combination with a shadowband. The shadowband is mounted below the sensor in an angle of (approximately) 45° and rotates continuously approximately once per minute around the sensor (see Figure 1). This way it is ensured that during rotation the shadowband once implies a shadow on the sensor, blocking out the sun for a short moment.

The irradiance measured over time during the rotation results in a typical measurement curve, which is called burst or sweep (see Figure 1).

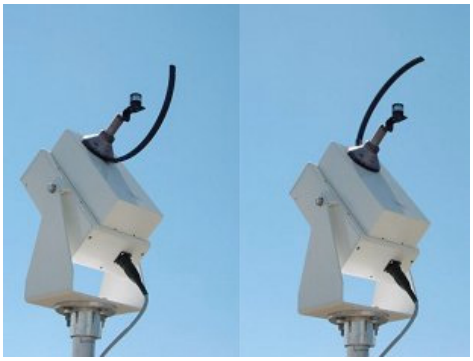

Figure 1: One example for a RSI: Rotating Shadowband Pyranometer (RSP) in normal position (left) and during rotation (right).

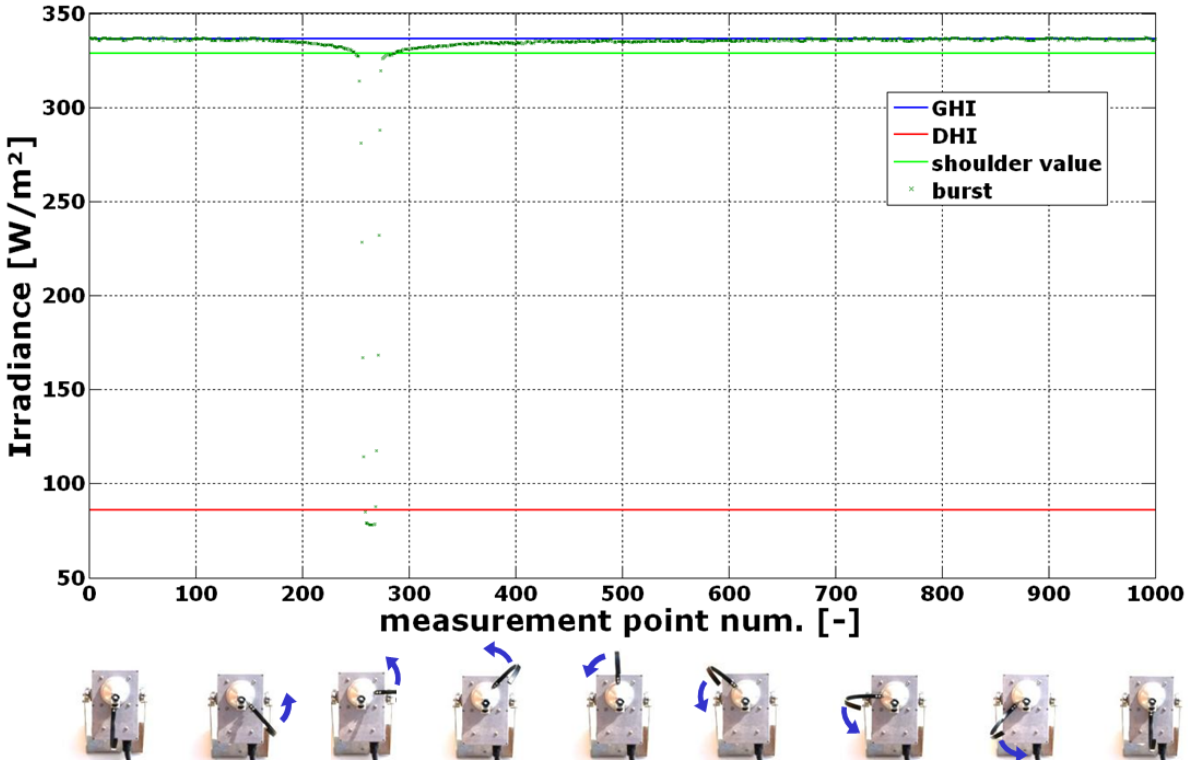

Figure 2: Burst (sweep) with sensor signal and the derived GHI, shoulder values and the DHI.

At the beginning of the rotation the pyranometer measures global horizontal irradiance (GHI). In the moment when the center of the shadow falls on the center of the sensor it basically only detects diffuse horizontal irradiation (DHI). However, the shadowband covers some portion of the sky so that the minimum of the burst is less than the DHI. Thus, shoulder values are determined and the difference between the average of the shoulder values and the GHI is added to the minimum of the curve to obtain the DHI. Subsequently direct normal irradiation (DNI) is calculated by the datalogger using GHI, DHI and the actual sun height angle by known time and coordinates of the location.

One version of such an algorithm defines the distance (in measurement points) between the positions of the minimum (p_{min}) and the maximum of the burst's slope as the well width (w_{well}). The position of the left shoulder value $p_{shoulder,L}$ is then defined as half the well width left of p_{min}:

$p_{shoulder,L} = p_{min} - w_{well}/2.$

The right shoulder value is found correspondingly. The shoulder value is the average of the left and the right shoulder value. The difference between the GHI and the shoulder value is added to the minimum of the curve to obtain the DHI. Finally, DNI is calculated using GHI, DHI and the sun height angle.

DHI and DNI are only determined approximately once or twice a minute, but GHI measurements can be sampled in a higher frequency without the rotation of the shadowband, e.g. every second. The variation of the GHI also contains some information about the change of DNI. Different algorithms are used to determine the minutely average of DHI and DNI from the burst and the more frequent GHI measurement. These algorithms are presented below in the descriptions of different existing RSI systems that are summarized in the next subsection.

The LI-COR radiation sensor is a practically instantaneously measuring device, but shows dependence on temperature and also lacks uniform spectral response in its sensitive range between 0.4 and 1.2 µm. As the whole range of incoming radiation lies between 0.25 and over 2.5 µm and its spectrum is varying with changing atmospheric conditions, this results in the mentioned low accuracy. Some mayor changes can be detected at low solar elevations when a significant part of the near infrared solar radiation is absorbed by water vapor. Calibration of the RSI radiation sensor has been carried out by the manufacturer against an Eppley Precision Spectral Pyranometer for 3 to 4 days under daylight conditions. Depending on the exact sky conditions during that period, a certain error of the determined calibration constant might occur. The calibration of the RSIs is required and corresponding methods are described later.

The most important specifications of the used sensor are listed in Table 1.

Main causes of the systematic deviations are the limited spectral sensitivity and temperature dependence of the SI-photodiode commonly used in most RSIs. The

corresponding correction functions have to be considered an essential part of the measurement instrument and are described later.

Table 1: Specifications of the used LICOR sensors.

	LI-COR
Response time (95 %)	10 µs
Zero off-set (T_{amb}-drift by 5 K/h)	—
Non-stability	< ±2 %/a
Non-linearity (<1000 [3000] W/m²)	±1 %
Temperature response (-10...+40°C)	±0,15 %/K
Directional response	< ±5 %
Calibration error (manufacturer calibration)	±3 ... ±5 %
Viewing angle	2π sr

2.1. Existing RSI instruments

Below are three examples of commercially available RSI instruments with continuous rotation. Please note, that the complete required system consists of the RSI instrument itself, a datalogger, that controls the instrument (rotation) in some cases and also the important correction functions for systematic errors. Specifications and distributors contact details are listed in Table 2, Table 3 and

Table 4. RSIs with discontinuous rotation are not described here due to their different principle of operation.

Table 2: CSPS Twin-RSI by CSP Services GmbH

Instrument name:	CSPS Twin-RSI
Manufacturer:	CSP Services GmbH
Contact:	n.geuder@cspservices.de
Homepage:	www.cspservices.de
Pyranometer type:	LI-COR LI-200
Sensor temperature measurement:	Yes
Datalogger:	Campbell Scientific (CR3000 / CR1000 / CR800 / ...)
Solar position algorithm:	Astronomical Almanac's Algorithm from J. J. Michalsky (Solar Energy Vol.40, No. 3, pp. 227-235, 1988)
sampling rate GHI:	1 / second
Rotation frequency:	1 / 30 seconds (alternating for the two sensors)
Method to derive DHI and DNI 1min averages from the measurement during the rotation:	DHI: shadowband correction for DHI measurements, averaged with preceding value DNI: calculated from GHI, DHI and solar position as 1-min average with correction for potential DHI drifts
Further remarks:	-set-up with two separately calibrated pyranometers for redundancy, high accuracy and reliability -rotation speed controlled shadowband enables additionally measurement of sunshape -application of DLR-post-corrections (spectral, instrument temperature, incidence angle, etc.) on raw measurement data to reach high measurement accuracies (~3 % RMSD instantaneous DNI, <2 % for annual DNI -lower soiling sensitivity due to redundancy -optionally analog output of irradiation valuese for systems without datalogger)

Table 3: RSR2 by Irradiance, Inc.

Instrument name:	RSR2
Manufacturer:	Irradiance, Inc.
Contact:	chris@irradiance.com
Homepage:	http://irradiance.com/
Pyranometer type:	LI-COR LI-200
Sensor temperature measurement:	No (ambient only, plus correction)
Datalogger:	Campbell Scientific CR1000, CR800
Solar position algorithm:	Campbell Scientific built-in (Michalsky)
sampling rate GHI:	1 / (5 seconds)
Rotation frequency:	At least 1 / (30 seconds), at most 1 / (5 seconds) if 20 w/m2 change in GHI
Method to derive DHI and DNI 1min averages from the measurement during the rotation:	Averaged after calculation of DHI/DNI for each rotation
Further remarks:	None

Table 4: RSP 4G by Reichert GmbH

Instrument name:	RSP 4G
Manufacturer:	Reichert GmbH
Contact:	http://www.reichertgmbh.de, info@suntrace.de, CSPS, S2M, GeoModel
Homepage:	www.reichertgmbh.de, www.suntrace.de, www.cspservices.de
Pyranometer type:	LI-COR LI-200
Sensor temperature measurement:	Yes
Datalogger:	Campbell Scientific CR800/CR1000
Solar position algorithm:	Campbell Scientific built-in (Michalsky)
sampling rate GHI:	1 / second
Rotation frequency:	1 / (60 seconds)
Method to derive DHI and DNI 1min averages from the measurement during the rotation:	DHI: calculated after rotation every minute, averaged every minute from two 1 minute samples (current value and value from last minute) DNI: calculated every second by 1 second GHI sample and 1 minute DHI sample, averaged every 60 seconds, corrected by correction factor, which is determined from two 1 minute samples of DHI and 60 seconds average of GHI
Further remarks:	spectral, temperature, angular correction and applying of 2, 3 or 4 calibration factors (GHI, DNI, DHI) in post processing

3. Measurement site selection

Selection of a good site that is representative of the surrounding environment is critical in order to obtain valuable and accurate meteorological measurement data. In general, the site should be representative of the meteorological conditions in the whole area of interest and should not be affected by obstructions like close hills, buildings, structures, or trees. Guidelines for site selection are contained separately for each measurement variable in the WMO Guide to Instruments and Measurements [WMO2008]. They are summarized and completed with a few practical recommendations in the following section.

3.1. General requirements

- Dimensions for the selected measurement site should be at least 10×10 m², with a recommended area free of obstructions of 25×25 m²
- Slopes should be avoided, a horizontal ground is desirable
- Accessibility by motor vehicle should be given in order to facilitate transportation, installation and O&M activities, while public access should be restricted or avoided. Preferably, a protection fence should be constructed around the site provided that it does not interfere with the sensors normal operation.
- Remote data transmission via mobile phone network, phone landline, ethernet or even radio frequency should be possible. Operators should check the communication options and in particular mobile phone network signal strength and integrity before final site selection. Where no other communication means are available, satellite data transfer might also be considered.
- Avoid power lines crossing the site, either underground or above ground. Other than to minimize the influence of shadows, this is for safety reasons in order to avoid electric shocks in case of touching the power lines, while it is also important to eliminate the influence of electric fields from alternating current power lines that might disturb the measurements by inducing noise signals in the cabling of the station. Contact local utilities for the location of buried utility lines

3.2. Additional requirements for the measurement of solar radiation

- The distance between radiation sensors and any obstacle should be at least 10 times the difference in height between the sensor and the obstacle.
- Above the plane of sensing, no obstruction should be within the azimuthal range of sunrise and sunset throughout the year; any obstruction above the horizon affects the measurements and leads to errors. On sites where it is not possible to avoid obstructions, the complete details of the horizon and any obstructions should be included in the description of the station to facilitate a subsequent assessment of their impact.
- No direct shade, artificial light or reflections from reflective surfaces should inflict the sensor at any time of the day and year.

- Avoid construction features that may attract roosting or nesting birds, otherwise the use of spike strips or other measures is recommended.

3.3. Additional requirements for co-located measurement of wind

- Wind towers should be set up in an azimuthal direction from the solar sensors where the sun never appears during the entire year in order to avoid shadows (i.e., to the north in the northern hemisphere and to the south in the southern hemisphere).

3.4. Locations that should be avoided

The operator is finally responsible for the selection of an adequate location for installing measurement stations. Even as the conditions of each prospective site are particular, some general recommendations can be established although the following list is not extensive:

- Low places where water might accumulate after rainfall or floods
- Erosion prone areas
- Large industrial areas
- Proximity to any emitting sources of dust, aerosols, soot or other particles
- Steep slopes
- Sheltered hollows
- Existing high vegetation or places with fast growing seasonal vegetation
- Shaded areas
- Swamps
- Areas with snow drifts
- Dry and dusty areas with a frequented road close by
- Irrigated agricultural land

3.5. Security and surveillance

To avoid theft or damage of equipment, the station should be properly monitored and protected by at least surrounding it by a fence as described below:

- The fence should be of enough height to avoid or discourage people and animals climbing over.
- The fence perimeter must be at a distance of at least twice the difference between instrument height and fence height with the irradiance sensor located at a higher level.
- It is recommended to secure a location within private property or property of public institutions.
- For security and surveillance reasons it is recommended to have local staff near the station that can control the station at regular intervals and can report possible vandalism, lightning damage, malfunction, etc. These intervals should be determined based on O&M needs, accessibility, funding, and other factors.

4. Measurement station hardware and installation

4.1. Power supply

For unattended remote sites, automatic weather stations must provide their own power source through a solar photovoltaic panel and a backup battery of proper capacity. The backup battery must be specified to supply at least the amount of energy needed by the system to ensure proper operation during the time that the maintenance team requires detecting and correcting the power supply failure, which should normally not exceed one week.

If the system does not provide its own power source but relies on an electrical connection it should be equipped with an UPS (uninterruptable power supply). The UPS should send an alarm when it starts providing backup power, so that the operation and maintenance personnel can react within the duration time of the battery.

4.2. Grounding and shielding

The equipment should be properly grounded to prevent lightning damage, and also shielded to prevent radio frequency interferences.

4.3. Communications, data transfer and storage

Manual download from the data logger is possible in most cases, although it is recommended that GPRS or 3G data transfer should be used in order to have access to the measurement system continuously or in daily scale. Alternatively, ethernet, WIFI or wired modem with internet access can be used if corresponding facilities are available; satellite communication could be an option (e.g. Iridium) in very remote areas. Regular manual download requires a high frequency of site visits in order to avoid any data loss due to data storage restrictions or malfunctions, and also for quick detection of measurement error and instrument malfunction.

4.4. Environmental conditions

Instruments, meteorological measurement stations and support structures must be able to withstand tough atmospheric and environmental conditions, requiring the lowest possible maintenance effort. Lightning damage protection, e.g. a grounding rod, should be foreseen. The equipment should be specified for at least a temperature range of -30°C to +55°C and high wind speeds, depending on the expected climate on site. All parts accessible from outside should be safe against bite damage by animals and made of stainless material to prevent corrosion. Cables and other equipment must be UV resistant. All mechanical parts and joints of the meteorological station must be capable to withstand wind, thermal, earthquake, and other natural stresses that should be identified before system deployment. Opportunities for bird and insect nesting within components should be minimized if possible.

4.5. Documentation of site and installation

The following documentation should be included with the measurement equipment:

- Layout diagram for the whole station area (within the fence)
- Drawings of required foundations, grounding poles and all other necessary civil works on the measurement site
- Installation and operation manuals for each device or sensor
- Listing of installed sensors with sensor specification, serial number, calibration protocol and history
- General station layout description and wiring diagram
- Maintenance instructions for high-quality data acquisition and transmission
- At the site of the meteorological station it is necessary to indicate basic emergency procedures and operator contact data to facilitate local staff reporting of any anomalous situation.
- Photographical documentation of the station, the instruments and station surroundings including 360º panorama photo from the position of the irradiance instrument after completing the installation of the station with free view of the station surroundings, from North over East to North (or alternatively 8 single photos towards: NN, NE, EE, SE, SS, SW, WW, NW)
- Optionally, web cams can be installed at the site in order to allow for visual inspection of the station (either as live view or from a memory card)

5. Operation and maintenance

A thorough operation of the meteorological station with regular maintenance of the equipment assures its proper functioning, reduces the effects of possible malfunctions thanks to early detection, and avoids or reduces the number and duration of data gaps.

5.1. General requirements

The maintenance personnel should keep a logbook in which normal and unusual events should be properly described. The technician attending the station must be trained to fill the logbook properly during each visit. Detailed information recorded in the logbook (see documentation list below) can be of the highest value if data quality issues arise. Events to be noted in the logbook are e.g. of insects, nesting birds or animals at short distance, occurrences of localized dust clouds (such as caused by traffic on a dusty road), haze or fog. Any abnormal events, the condition of the instruments, infrastructure and environment should be documented on any occasion when such observations have been made. Pictures with date/time stamps are useful for this purpose and provide a valuable visible insight on the conditions of instruments. The horizontal level of the instruments should be checked each time, particularly if their pedestal or the ground around it shows signs of alteration or erosion.

Instrument maintenance and operation should only be performed by qualified, trained personnel. The frequency and extent of maintenance visits also depends on the instrumentation and site characteristics, and requires careful consideration during the planning stage of the measurement campaign. The cost of maintenance during a long-term measurement campaign can easily exceed the initial cost of the instrumentation. The planned cost of operation and maintenance has to be considered in the budgetary framework, and additional provisions should be made in order to face any unexpected malfunction.

5.2. Prevention from power outages

The equipment should be protected from power outage by providing an uninterruptable power supply (UPS), which also needs regular check-up. Since the efficiency of UPS batteries tends to degrade over time and under severe environmental conditions, they must be tested at regular intervals (e.g., every 6 months or even shorter intervals) and replaced if necessary.

5.3. Instrument cleanliness

RSI instruments are not as prone to soiling effects as other radiation sensors such as pyrheliometers. Nevertheless, they require regular cleaning. The cleaning interval should be defined as site-specific at the beginning of the measurement period by analyzing the immediate effect of cleaning on the measurement signal. Depending on how the noted period after which the sensor soiling remarkably influences the measurement, the cleaning interval should be adjusted in a way that soiling

effects are never bigger than as to cause a 1-2 % degradation in sensitivity. Each cleaning and the state of the sensors should be documented and the measurement values should be checked to evaluate the effect of cleaning on the recorded values. Taking photographic records of the sensor with time/date stamps before and after the cleaning events is recommended.

5.4. Instrument alignment

Pyranometers and photodiodes measuring global and diffuse radiation must be leveled accurately, especially if the main interest of the measurement is the determination of DNI. Any misalignment has to be avoided and needs to be rapidly detected, corrected and documented. Accurate horizontal alignment of sensors should be checked regularly using a spirit level with at least 35 arc minutes sensitivity. Here 35’ is related to a displacement of the bubble by 2 mm relative to the case of the spirit level and not to the maximum error of the levelling which is much lower than 35’. The levelling error should be below 0.1°. Depending on the RSIs leveling mechanics and the stability of the RSI’s mount also a 5’ can be recommendable. Spirit levels present in some sensors are a quick indicator of inclination but do not provide accurate sensitivity but should not be used as only device to level the irradiance sensor. A separate spirit level should be set on the LI-COR sensor and checked for the correct horizontal alignment in two rotational azimuthal orientations: first in an arbitrary orientation of the spirit level and then with the spirit level rotated around its azimuth axis by 180° in order to compensate potential imperfection of the spirit levels ground plate. Note that the ideal horizontal adjustment will not result in a perfectly centric position of the bubble within the spirit level if the spirit level itself is not perfect. For such a perfect alignment and an imperfect spirit level the bubble will not be exactly in the center of the bubble, but it will not change its position relative to the case of the spirit level when rotating the spirit level by 180°.

Furthermore, the shadowband has to be aligned in its rest position pointing to Geographic North in the Northern Hemisphere and to Geographic South in the Southern Hemisphere. It has to be considered that Geographic North is not Magnetic North. Depending on the region deviation between Geographic North from the Magnetic North can reach around 30º. The precision of the shadowband alignment to North is not so strict but should not exceed an angle of approximately 5º.

5.5. Data collection and analysis

For high quality and reliable measurements, it is recommended to ensure automatic data collection through a suitable communications system, and also perform regular (e.g. daily) screening for measurement failures and evaluation of data quality. Malfunctions have to be detected as soon as possible to avoid longer periods with data loss or defective data, respectively.

For the post processing of the measurement data an adequate quality assessment, flagging and gap filling method should be applied to generate high quality and gap-

less data sets. Continuous time series without gaps are required since the most applications, like models for plant performance simulations, require gap less data sets. Appropriate automatic procedures for quality assessment and gap filling are topics in IEA Task 46, Subtask B2 and several publications ([Long2002], [Maxwell1993], [Wilcox2011], [Journee2011], [Espinar2011], [Geuder2014]). In addition to automatic procedures further visual inspection by an expert is required as automatic procedures cannot detect all erroneous data and some correct data points might be flagged by error. Visual inspection of the data allows the detection of measurement. Specialized data acquisition and quality management software exists (e.g. [Geuder2014]). A procedure for analysis and correction of soiling effects should be included in the analysis software and explained to the local personnel in charge for the regular inspections and sensor cleaning.

Optional redundant measurements can be of great help for data quality assessment and can increase data reliability and availability. In addition to an RSI a second RSI, a second thermal pyranometer, an additional LI-COR pyranometer, satellite derived data and nearby other measurement stations can be used.

5.6. Documentation of measurements and maintenance

Required documentation:

- Written maintenance procedure for station keeper with exact formulation of tasks to be done
- Date and time of sensor cleaning by station
- Special occurrences with date, time and description (sensor or power outages, …)
- Gaps and eventually gap filling method with corresponding information
- Correction procedure/method for irradiance data
- Proceeded data processing and quality control procedure
- Changes of the instrumentation or the surroundings of the station require updates of the documentation listed in the previous section.

Recommended documentation

- Electronic documentation whenever possible
- If possible additional button to be pressed at sensor cleaning for leaving an electronic entry in the data set

6. Corrections for RSI irradiance measurements

6.1. Spectral, cosine response and other systematic errors of the LI-200 pyranometer

The photoelectric effect is quantitatively described by Equation 1, Equation 2 and Equation 3.

$$\phi = h \cdot f_0 \qquad \textit{Equation 1}$$

$$hf = \phi + E_{k,\max} \qquad \textit{Equation 2}$$

$$E_{k,\max} = \frac{1}{2} \cdot m_e \cdot v_m^2 \qquad \textit{Equation 3}$$

Φ: Minimum energy required to remove a delocalized electron from the band
$E_{k,max}$: Maximum kinetic energy of ejected electrons
h: Planck's constant
f: Frequency of the incident photon
f_0: Threshold frequency for the photoelectric effect to occur
m: Rest mass of the ejected electron
v_m: Velocity of the ejected electron

The equations imply that if the photon's energy is less than the minimum energy Φ, no electron will be emitted since an emitted electron cannot have negative kinetic energy. If the photon has more energy than Φ this energy will partly be converted to kinetic energy and not to electric energy. The spectral response is the part of the photon's energy that can be converted to electric energy. It is typically given relative to its maximum. The response of photoelectric pyranometers is not the same for all wavelengths within the solar spectrum as it is seen in Figure 3, which illustrates the spectral response of the LI-200 pyranometer. The sensor only responds to wavelengths between 0.4 and 1.2 µm. Its spectral response within this interval is not uniform. The response to blue light is noticeably lower than for red light and colorinfrared radiation. This inhomogeneous spectral response causes a spectral error of the broadband irradiance measurement.

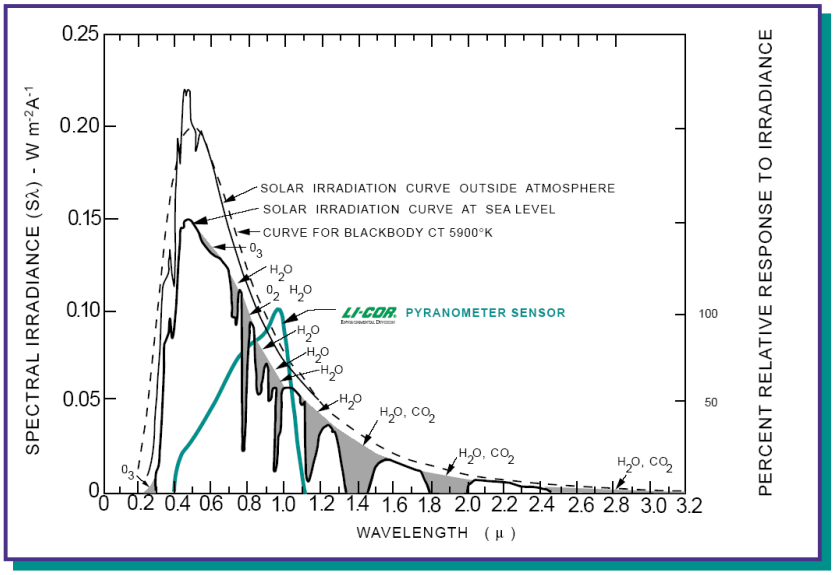

Figure 3: LI-200 pyranometer spectral response along with the energy distribution in the solar spectrum, [Biggs2000]

Although the LI-200 Pyranometer is said to be a fully corrected cosine sensor, according to [Biggs2000] it has a typical cosine error of up to than 5 % up to an 80° angle of incidence, as it is seen in Figure 4. At 90° angle of incidence a perfect cosine collector response would be zero, and at that angle any error is infinite. Totally diffuse radiation introduces a cosine error of around 2.5 %. For a typical sun plus sky at a sun elevation of 30°, the error is approximately 2 %.

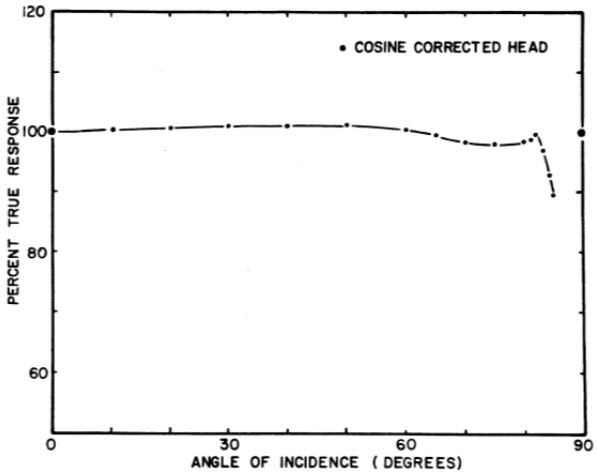

Figure 4: Cosine response of LI-COR terrestrial type sensors, [Biggs2000]

As almost every silicon photo cell, the signal of the LI-COR sensor has a temperature dependence in the order of 0.15 %/K.

The LI-200 azimuth error is less than ±1 % at 45°. The type of silicon detectors used in LI-COR sensors has a linearity error of less than ±1 % over seven decades of dynamic range. The stability error of LI-COR sensors is stated to be ±2 % per year in [Biggs2000]. Recent studies show lower drifts as described in section 7.3. The absolute calibration specification for LI-COR sensors (GHI measurement) is

conservatively stated ±5 % traceable to the NBS (U.S. National Bureau of Standards).

Although temperature and cosine responses of photodiode pyranometers have been well documented, the accuracy to which these systematic errors be characterized is somewhat influenced by the spectral response as the spectral distribution changes over the day, time of year, and location.

Several research groups have developed correction functions that reduce the systematic errors of RSIs.

Whereas temperature correction is widely coincident in all versions, the methods for the spectral effects vary between the publications. Due to the connection between the solar spectrum and the solar elevation, spectral corrections and incidence angle corrections are connected.

Different approaches for the spectral corrections are listed in the following. [Alados1995] uses tabular factors for different sky clearness and skylight brightness parameters and a functional correction depending on the incidence angle. [King1997] proposes functional corrections in dependence on airmass and the angle of incidence derived for global irradiation. This approach was further developed by [Vignola2006] including also diffuse and subsequently direct beam irradiance. Independently, a method was developed by the German Aerospace Center (DLR) using functional corrections including a particular spectral parameter composed from the irradiance components of global, diffuse and direct irradiance in 2003 and improved in 2008 [Geuder2008]. Additional corrections in dependence on airmass and incidence angle were used.

After application of the correction functions in comparing measurement campaigns, a comparable accuracy of RSI measurements was stated for annual scale as reached with properly maintained high-precision instruments like pyrheliometer [Geuder2010]. However, still remaining aspects are stated in [Geuder2010] and [Myers2011], calling for further improvements of the corrections. The most relevant corrections will be presented in this chapter.

6.2. Corrections by King, Myers, Vignola, Augustyn

King, et al., Augustyn et al. and Vignola developed and published different versions of correction functions for the Si-pyranometer LICOR LI-200SA [LICOR2005] that is used in all currently existing RSIs with continuous rotation.

The corrections depend on the sensor temperature, the solar zenith angle, the air mass (AM), DHI and GHI. In the presented version of the correction functions the GHI is corrected in the first step as described in section 6.2.1. The corrected GHI is then used for the calculation of the corrected DHI (section 6.2.2). Finally the corrected values for DHI and GHI are used together with the zenith angle to determine the DNI.

6.2.1. GHI Correction by King and Augustyn

The presented correction for GHI consists of work published in a series of publications. The first part of the corrections were published in [King1997]. One year later, King et al. published an update of their work in which some of the coefficients of the correction functions are given with more digits [King1998]. Later, Augustyn added one further correction factor based on these publications in [Augustyn2002]. In 2004, an update of this work was presented, in which the coefficients were given with more digits [Augustyn2004]. This document presents one complete set of GHI correction functions that is selected using the different available publications.

The selected correction makes use of four parameters

- F_α: the temperature parameter
- F_A; the spectral response parameter
- F_B: the cosine response parameter and
- F_C: the cat ear parameter

and is formulated as

$$GHI_{corr} = GHI_{raw} \cdot \frac{F_\alpha}{F_A F_B F_C} \qquad \textbf{Equation 4}$$

[Augustyn, 2004] with the uncorrected (raw) GHI (GHI_{raw}) and the corrected GHI (GHI_{corr}).

The four parameters of the correction are determined with the following formulas:

- F_α (temperature correction by [King1997]; with the coefficient of temperature dependence $\alpha = 8.2 \cdot 10^{-4}$ and the reference temperature T_{ref} = 25°C; T_{LICOR} also in °C)

$$F_\alpha = 1 - \alpha \cdot (T_{LICOR} - T_{ref}) \qquad \textbf{Equation 5}$$

- F_A (spectral response correction by [King1998]; with airmass *AM*)

$$F_A = 2.631 \cdot 10^{-4} \cdot AM^3 - 6.319 \cdot 10^{-3} \cdot AM^2 + 5.401 \cdot 10^{-2} \cdot AM + 0.932$$

Equation 6

- F_B (cosine response correction factor by David King [King1998]; solar zenith angle SZA in degree):

$$F_B = -4.504 \cdot 10^{-7} \cdot SZA^3 + 1.357 \cdot 10^{-5} \cdot SZA^2 + 6.074 \cdot 10^{-4} \cdot SZA + 1$$

Equation 7

- F_C (cat ear correction by Augustyn [Augustyn, 2004] (solar zenith angle *SZA* in degree)):

$$F_C = \begin{cases} 10.164664 - 0.24242 \cdot SZA + 1.603 \cdot 10^{-3} \cdot SZA^2 & ; \quad 75° < SZA < 81° \\ -58.03442 + 1.457577 \cdot SZA - 8.99 \cdot 10^{-3} \cdot SZA^2 & ; \quad 81° \le SZA < 83.2° \\ 1 & ; \quad 0° \le SZA \le 75° \vee SZA \ge 83.2° \end{cases}$$

Equation 8

In the case of absence of direct temperature data from within the pyranometer, T_{LICOR} can be estimated by following equation of unknown source.

Estimated pyranometer temperature in °C:

$$T_{LICOR} = T_{air} + (-4.883 \cdot 10^{-6} \cdot GHI_{raw}^2 + 0.00953 \cdot GHI_{raw} - 0.5) \qquad \textbf{Equation 9}$$

Figure 5 illustrates the estimation of the temperature dependence and its coefficient α by linear regression.

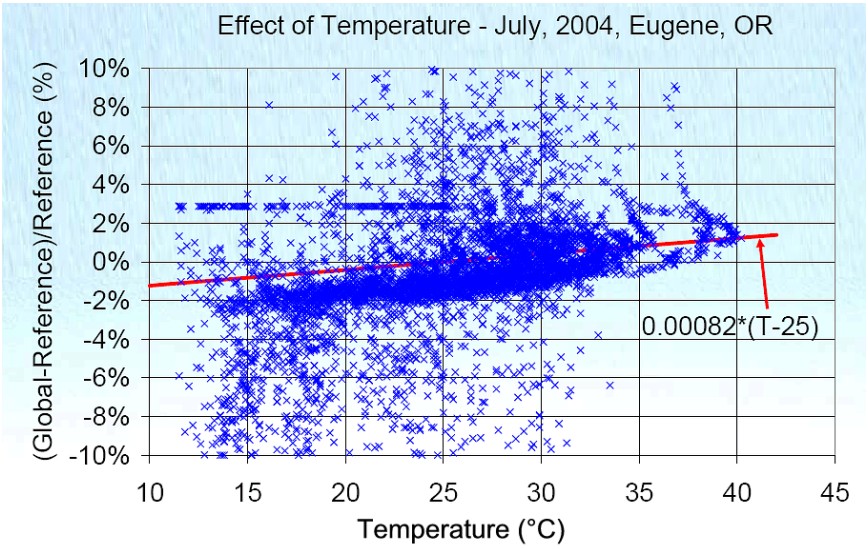

Figure 5: Temperature dependence on LI-COR 200SZ pyranometer, Courtesy of F. Vignola.

The above stated functions are used e.g. at DLR-PSA for the calibration of RSIs. It should be mentioned that other versions of the correction exist due to the deviations between the different published versions of the corrections. A summary of these deviations is given in the following. [Vignola2006] presented a new version of the global corrections, with an updated spectral correction (F_A) that closely matches the results for F_A obtained using the formula from [King1998], but fits the results better for high *AM* according to [Vignola2006]. The expressions for F_A and F_B in [Vignola2006] are the same as the ones given above from [King1998]. For F_C and zenith angles between 75° and 81° one coefficient in [Vignola2006] deviates from [Augustyn2004] and unrealistic results are obtained with the value from [Vignola2006]. For the other range of zenith angles the coefficient in front of *SZA* deviates by less than 0.2 % from the corresponding coefficient from [Augustyn2004]. This small deviation cannot be explained or excluded by comparison to reference irradi-

ance data, but it can be assumed that the deviation from the values given in [Augustyn2002] and [Augustyn2004] is by error.

In [King, 1997b] the coefficient in front of SZA in Eq. Equation **7** for F_B is given as $6.074 \cdot 10^{-5}$ instead of $6.074 \cdot 10^{-4}$. As $6.074 \cdot 10^{-4}$ is used in all other publications it can be assumed that $6.074 \cdot 10^{-4}$ is the correct coefficient.

The Cat Ear Correction was implemented in order to deal with the increase of inaccuracy at zenith angles above 75° which peaks at about 81° as shown in Figure 6 and Figure 7.

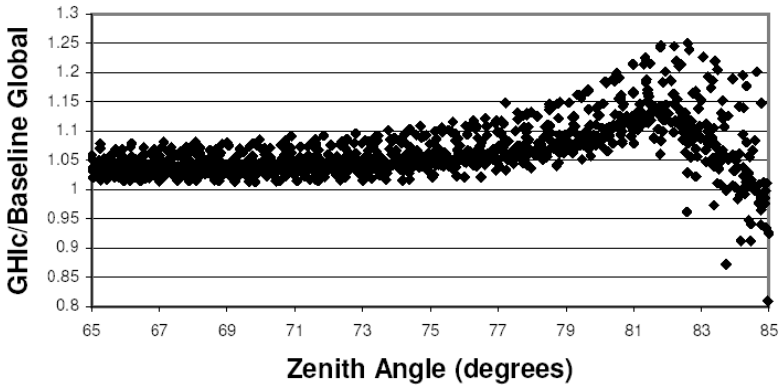

Figure 6: NREL GHI_{corr}/baseline GHI from 65-85° Zenith Angle: The Cat Ear error [Augustyn2002]

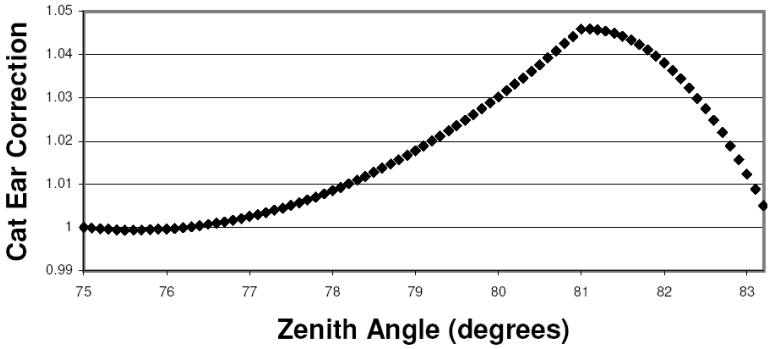

Figure 7: Cat Ear Correction [Augustyn2002]

6.2.2. DHI correction by Vignola et al (2006)

The applied version of Vignola's diffuse correction makes use of the corrected GHI and the uncorrected DHI. For $GHI_{corr} \leq 865.2$ W/m² the correction is performed as

$$DHI_{corr} = DHI_{raw} + GHI_{corr} \cdot (-9.1 \cdot 10^{-11} \cdot GHI_{corr}^{3} + 2.3978 \cdot 10^{-7} \cdot GHI_{corr}^{2} \ldots \ldots - 2.31329234 \cdot 10^{-4} \cdot GHI_{corr} + 0.11067578794)$$

Equation 10

For higher GHI_{corr} the correction is expressed as

$$DHI_{corr} = DHI_{raw} + GHI_{corr} \cdot (0.0359 - 5.54 \cdot 10^{-6} \cdot GHI_{corr})$$

Equation 11

The diffuse correction has been published in different versions in [Vignola1999], [Augustyn2002], [Augustyn2002] and [Vignola2006]. The first work by Vignola presented a correction for GHI > 100 W/m² that was later only used for high GHI levels (> 865.2 W/m²). The following two publications ([Augustyn2002] and [Augustyn2004]) used another formula developed by Vignola in the meanwhile for GHIs below this value. Furthermore they applied the correction using uncorrected GHI as variable. [Vignola2006] works with the corrected GHI and states that the corrections were developed for use with high quality GHI measurements and that they still work with corrected GHI values from RSIs. Thus the presented diffuse correction works with the corrected GHI signal. In [Vignola2006] a small deviation in one of the coefficients for the diffuse correction with GHI ≤ 865.2 W/m² appears. The change is less than 0.001 % and the value stated in [Augustyn2002] and [Augustyn, 2004] is used above.

With increasing GHI the diffuse error of the unrectified DHI value increases significantly in comparison to the corrected DHI. This correlation is illustrated in Figure 8.

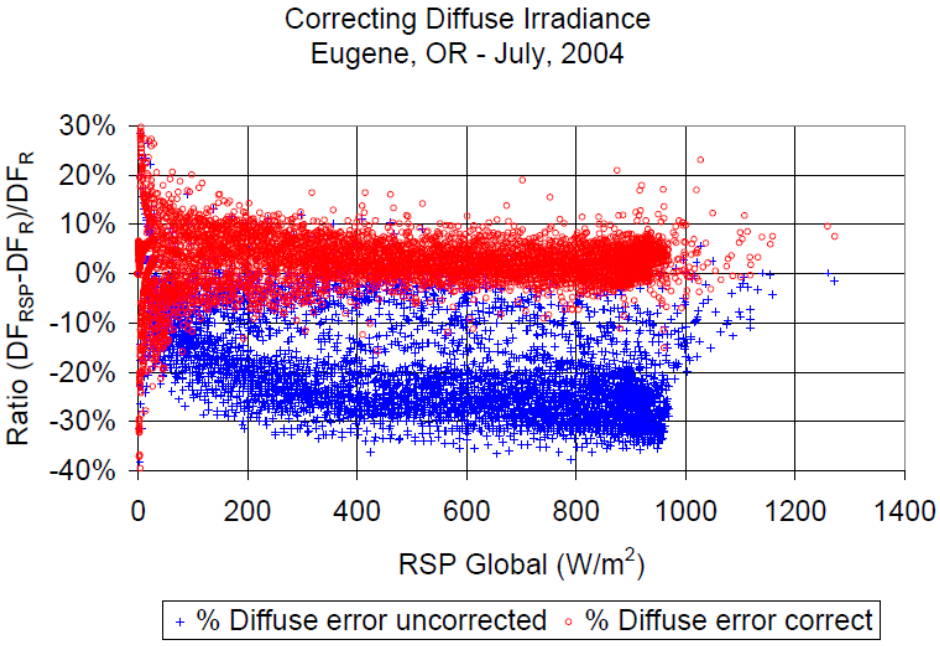

Figure 8: Comparison of DHI_{raw} (here DF_{RSP}) and DHI_{corr} (here DF_R) against GHI_{raw} (here RSP Global) [Vignola2006]

6.3. Corrections by Batlles, Alados-Arboleda, etc.

Previously a different approach to DHI correction was published by Batlles and Alados-Arboledas [Batlles1995]. It included the use of tabular factors for different sky clearness and sky brightness parameters and a functional correction depending on the incidence angle. Sky clearness and sky brightness are considered functions of cloud conditions and the presence of aerosols respectively. The first is derived from DNI_{raw} and DHI_{raw}, while the latter is determined by DHI_{raw}, the solar zenith angle and the extraterrestrial solar irradiance. The correction factor is then calculated

with linear regressions for different ranges of sky brightness, which is the second most significant parameter in this model after the solar zenith angle.

While the [Batlles1995] method focusses on sky conditions, the later developed DHI correction by [Vignola2006] as presented in section 6.2.2 produced higher accuracy by using a corrected GHI value on the basis of temperature, spectral influences and solar zenith angle instead of sky conditions and solar zenith angle.

6.4. Corrections by DLR

Among the systematic deviations of semiconductor sensors are primarily the dependence on the sensor temperature and the non-uniform sensitivity of the sensor to radiation from the entire solar spectrum. Their characteristic dependencies and corrections will be presented in the following.

For the derivation of correctional functions, the quotient of the precise reference irradiance to the corresponding RSI signal was calculated for every data point (available time resolutions were 1 and 10 minutes, respectively). This quotient represents the (running) correction factor CF_r to correct the measured RSI value in order to receive the true irradiance. It must meet as close as possible to a value of "1.0" after the corrections. Data sets of 23 different RSI were used within the evaluation, taken within a period of an entire year (June 2007 to June 2008). This allows for deduction of statistically solid mean values including seasonal variations of atmospheric conditions and the corresponding sensor response. As the raw RSI irradiation was determined just with the original LI-COR calibration factor, each data set was corrected for this imprecise calibration with a draft constant correction previous to the derivation of the functional coherences.

6.4.1. Correction of the temperature dependence

Generally, the temperature dependence of the LI-COR sensor is given by the manufacturer in its specifications to 0.15 %/K [LICOR2005]. More detailed investigations with multiple sensors showed a value of 0.00082 ± 0.00021 per Kelvin [King1997]. Measurements on RSI temperature dependence were performed with two different methods by DLR at the PSA:

- Measuring the sensor signal under real sky conditions (around solar noon) and temperature inside the sensor head while it was warming up from 0°C to around 40°C.
- Measuring the sensor signal and temperature under artificial illumination (a stabilized lamp) when the sensor was cooling down from 60°C to 5°C.

In both cases the signals of two reference photodiodes at constant temperature were used to eliminate minor variations of irradiation during the measurement. Both methods yielded nearly the same factor of 0.0007/K for the temperature dependence of the LI-COR sensor head in agreement with the value given by [King1997]. Figure 9 shows this dependence of the correction factor on temperature as gained from the measurements under real sky conditions. The response of

the LI-COR sensor is overestimating the true value at high temperatures and underestimating it at low temperatures. Therefore, the sensor response at e.g. 1000 W/m² may vary more than 30 W/m² depending on its temperature in winter or summer, where a difference of 40°C can easily be reached.

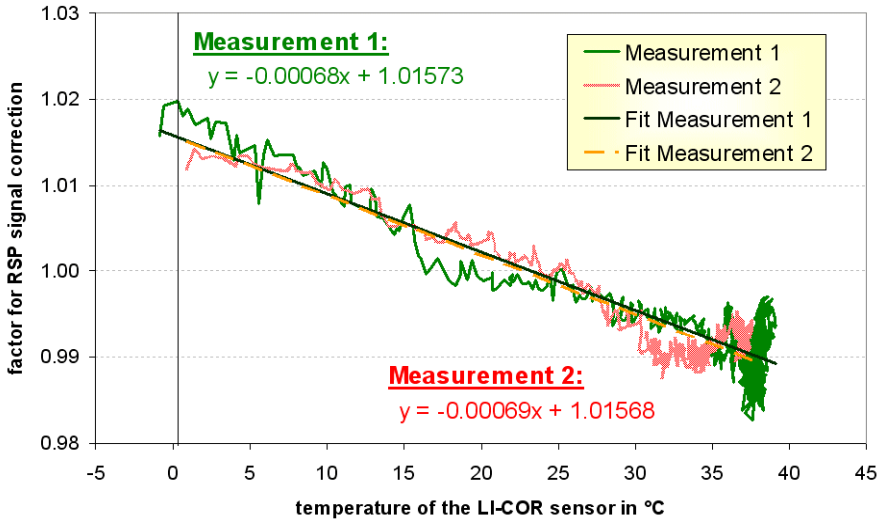

Figure 9: Dependence of the LI-COR sensor response on temperature

Performing a final parameter variation of the temperature coefficient within the correctional functions, we stated a marginally better correlation of the RSI correction to the reference data with a value of 0.0007. Therefore we agreed on using that value. As a common reference temperature, the value of 25°C was chosen. Finally, the factor for correcting the temperature influence is calculated along:

$$C_{temp} = (1 - 0.0007 \cdot (T_{LI-COR} - 25°C)) \qquad \textbf{Equation 12}$$

A feature of the RSI instruments from Reichert GmbH and from CSP Services is the additional temperature probe in its sensor head. The sensor temperature differs significantly from ambient temperature depending on its heat exchange with the environment. Using ambient temperature for corrections can lead to an additional error in the sensor response of approximately 10 W/m² depending on actual irradiation, wind velocity and the concurrent IR radiation exchange between atmosphere, ground and the sensor head.

6.4.2. Spectral influence on diffuse irradiation

One major influence especially on the diffuse irradiation is the non-uniform spectral response of the semiconductor sensor. It reaches its maximum sensitivity in the near infrared decreasing slowly to 20 % of this value at around 400 nm and more steeply towards longer wavelengths as shown on the right chart of Figure 10. Therefore, the clearer the sky and the higher the blue portion of the diffuse irradiation from the sky, the more it underestimates the true DHI value (at very clear, deep blue skies maybe half the signal).

To obtain a suitable parameter to correct this spectral dependence, various parameters including e.g. sky clearness parameter and skylight brightness parameter as well as further numerous combinations of accessible measured values were analyzed. In the correction algorithm developed formerly by DLR [Geuder2003], a linear dependence on the quotient of direct-normal to diffuse-horizontal (DNI/DHI) was used. There the distribution of the values around the functional curve was rather wide. By further examinations, we now achieved to find a parameter with a narrower spread of the CF_r around the main curve (see Figure 10). This spectral parameter – called Π_{spec} – which yield the narrowest spread, is calculated along:

$$\Pi_{spec} = DNI \cdot GHI / DHI^2 \quad . \qquad \textbf{Equation 13}$$

Analyzing successively the CF_r of all data sets against Π_{spec}, a variation of its maximal values was detected, showing a seasonal variation. This reflects the changing atmospheric conditions in southern Spain throughout the year: in winter and early spring maximal DNI values are obtained at very clear skies and in summer generally lower DNI at increasingly hazy and turbid atmospheres are observed. The correlation between the CF_r and the spectral parameter finally is described by a functional correlation with a linear and an exponential term with Π_{spec} as variable and its coefficients linear functions of the ambient temperature.

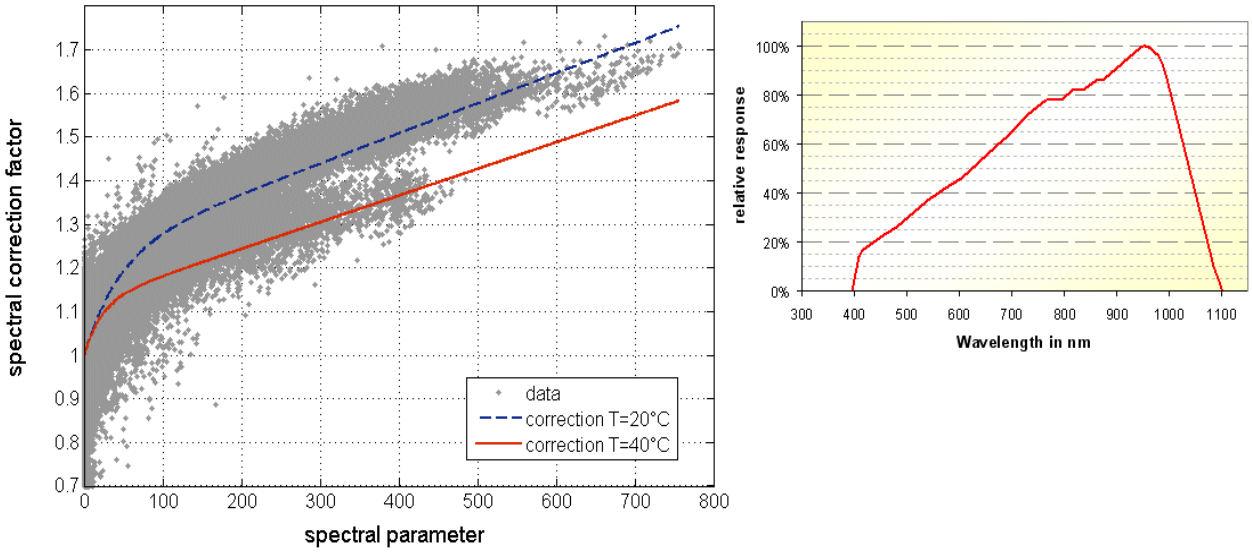

Figure 10: Correlation between the Correction Factor of diffuse irradiation and the spectral parameter Π_{spec} = DNI·GHI / DHI² and dependence on the ambient temperature (left) and spectral response curve of the LI-200SA sensor head (right) [LICOR].

The impact of the spectral correction can clearly be seen comparing original and spectrally corrected DHI in the right graph of Figure 11: the uncorrected raw DHI has a clear peak up to values of 1.8 at small Air Mass Factor (AMF), which disappears with the spectral correction.

As the diffuse fraction of global irradiation is also affected by this spectral error, its influence on the global irradiation was analyzed, too. Although a minor improve-

ment could be detected at certain GHI intensities with a spectral correction applied, the overall correlation performed better without.

6.4.3. Correction of Air Mass dependence

The Air Mass Factor (AMF) is used for another correction automatically including the altitude of the location. AMF is calculated along [Young1994], pressure-corrected with measured values or – in absence of measurements – calculated via the international height formula, including ambient air temperature. The true solar zenith angle (without refraction), necessary here for calculation of AMF, is determined along an algorithm of [Michalsky1988].

The yet spectrally corrected CF_r of DHI in the left chart of Figure 11 are located within a clearly delimited band at small AMF values (high solar elevations) within values of 0.8 and 1.2, smoothly decreasing with rising AMF (lower solar angles) and with a rising spread of the values. The mean curve could be well approximated with function of a quadratic and a linear term in dependence of the AMF and was fitted to the spectrally corrected DHI.

The running correction factors of the GHI RSI data also show dependence on the air mass factor. However to see the correct correlation, previously the influence of direct beam response at low sun elevations (described in section 6.4.4) has to be eliminated in analogy to the spectral factor at DHI. Without the direct-beam influence, a similar smooth dependence of global CF_r on the AMF emerges (see left graph in Figure 11) and is corrected along the same functional correlation with just different coefficients.

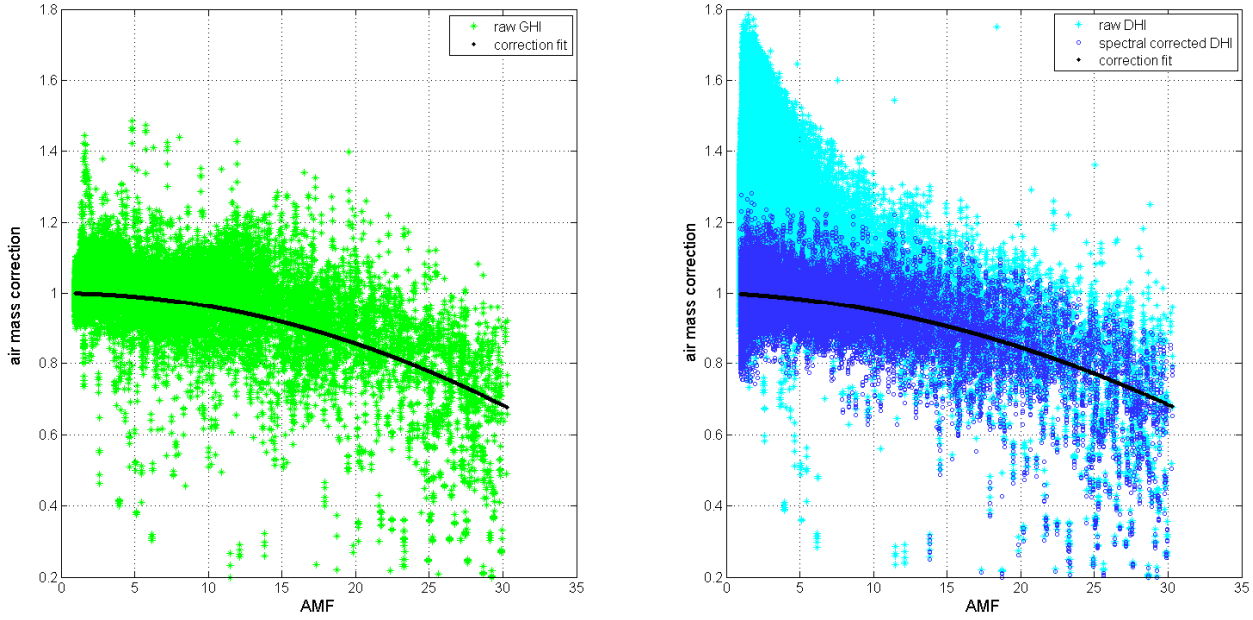

Figure 11: Correction of the RSI response in dependence on the pressure-corrected air mass factor AMF for global horizontal irradiation (left) and diffuse horizontal irradiance (right) with and without spectral correction.

6.4.4. Correction of the directional response of the LI-COR sensor in dependence on the incidence angle

Vice versa eliminating the influence of air mass from the global CF_r values, a characteristic dependence on the incidence angle turns up. The response is affected in particular at incidence angles beyond 75 degrees. High incidence angles here correspond to low solar elevations as in our case the sensor is always mounted horizontally. Unfortunately the overall accuracy is poor at high incidence angles in combination with the non-ideal cosine correction and maybe non-ideal leveling as well as moreover here due to usually small irradiation intensities. Therefore a mean curve of the AMF-corrected global data was determined here from the cloud of widely spread values to visualize the dependence. The mean curve of the data is plotted in Figure 12 together with the fit of the correction function. The exact form of the mean curve is varying slightly among the various data sets supposedly due to minor variations in mounting and assembly of the LI-COR sensor as well as maybe also due to seasonal/spectral effects. However, its characteristic form is similar among all data sets and is known as the "cat-ear" effect [Augustyn2004]. The reason for this effect must be linked to the way the direct beam hits and penetrates the small white diffuser disk, which is covering the semiconductor sensor.

The developed correction function represents the sum of an exponential and a combined sinusoidal and exponential term with the solar elevation as variable for solar elevations over 3 degrees and a steadily connected linear function for lower solar height angles.

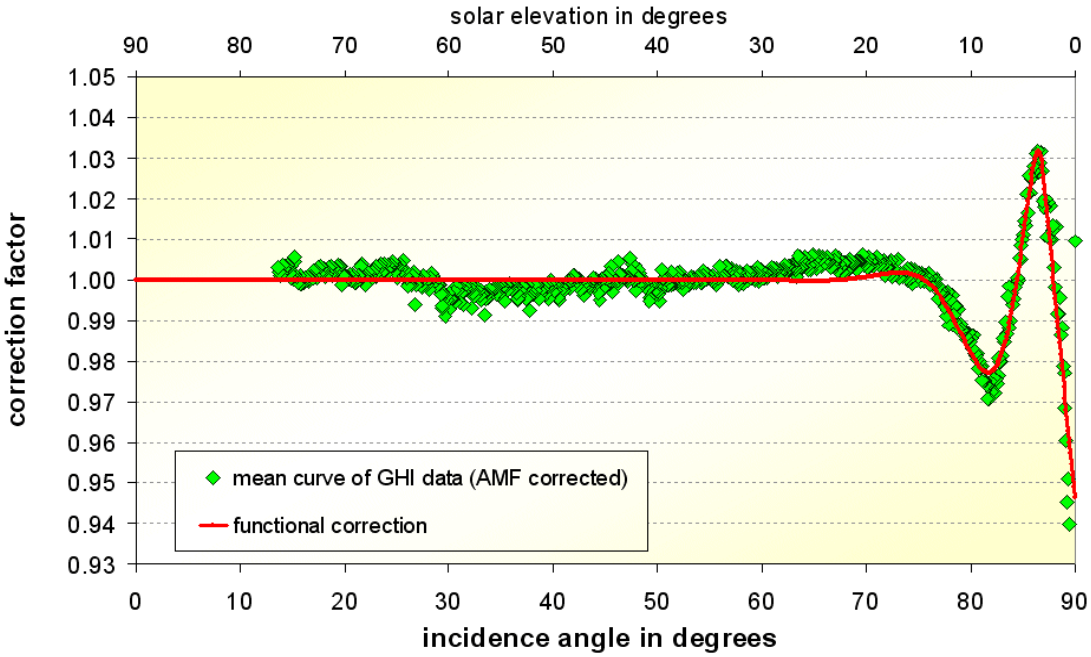

Figure 12: Mean curve of (AMF-corrected) CF_r of global horizontal irradiation in dependence on the angle of incidence

6.4.5. Correction of remaining errors: intensity and constant factor

Analyzing the remaining deviation between the corrected RSI response and the reference values, just some minor systematic deviations were visible for diffuse and direct normal irradiance in dependence on their intensity. The diffuse irradiation was marginally overestimated for intensities over 350 W/m², which is corrected with an additional cubic function on DHI. The remaining deviation of DNI could be corrected with a linear function on its intensity. No further systematic deviation could be stated for any available parameter; however raising values of relative air humidity generally increased the measurement error.

With finally all former presented corrections applied, new constant correction factors CF were determined for each RSI separately for global and diffuse irradiation. The correction factors and functions refer to the original calibration factor from LI-COR Inc. From the 23 analyzed RSIs, we got an average constant *CF* of 1.023 for global irradiation and 1.32 for diffuse irradiation with corresponding standard deviations of 0.9 % and 1.4 %, respectively. The variability of the *CF* values is illustrated in Figure 13 separately for GHI and DHI. The y axis represents the relative deviation of each *CF* to the denoted average values.

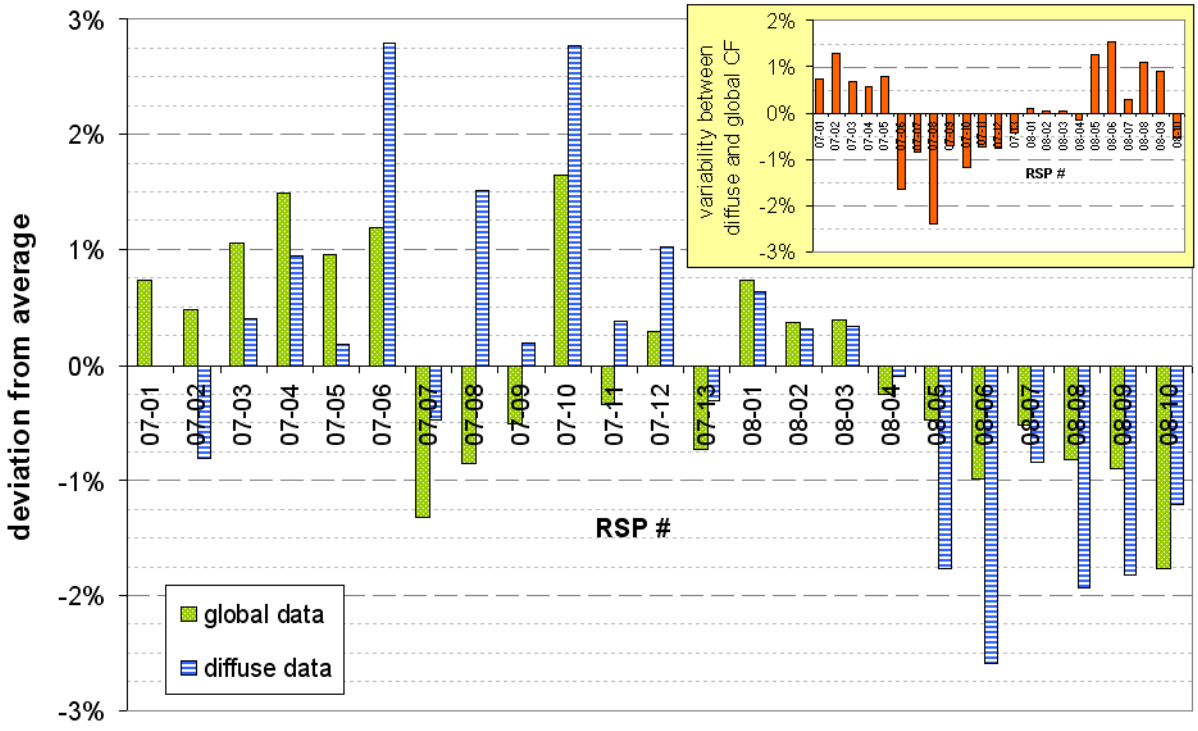

Figure 13: Variability of the constant Correction Factor CF for global and diffuse irradiation data, plotted as relative deviation to the average CF of the analyzed Reichert GmbH Rotating Shadowband Pyranometer. The slide-in chart at the top shows the variability between the global and diffuse CF.

For single sensors maximal deviations of 3 % from the mean value were found for diffuse and below 2 % for global irradiation. However, in addition to the variability of the constant factors among different RSIs, the quotient from the global and dif-

fuse correction factor is neither constant but varying within 2.5 % (on average: 1.1 %). This variability is not corresponding to seasonal variations nor could other obvious reasons be stated. Thus we suppose intrinsically differences, for example the spectral sensitivity. Finally two separate correction factors shall be determined at the calibration for global and diffuse irradiation. As the focus of measurements with RSI irradiation sensors is usually the determination of DNI, the main calibration factor for global irradiation will be calculated by scaling the corrected DNI response to the reference values. The loss of accuracy for global irradiation is negligible as the difference is usually even within the accuracy of the precise reference sensors.

6.5. Corrections by CSP Services

With ongoing calibration of RSIs by DLR since meanwhile nearly 10 years and operation of RSIs in several continents, altitudes and climate zones, a comprehensive data set is available for analyzing the LI-COR sensor response and its systematic deviations. For the development of enhanced corrections, 39 different RSIs at different sites and climate zones have been examined, based on data over a range of 2 years. Besides the thorough analysis of field measurements, theoretical examinations have been performed about spectral dependencies of the irradiation components and practical experiments conducted on angular dependencies of the LI-COR pyranometer sensor. Finally, the following correlations are elaborated:

6.5.1. Correction of Diffuse Horizontal Irradiance:

On clear days, a large part of the Diffuse Horizontal Irradiance (DHI) originates from the short-wave (blue) wavelength range; this proportion however changes drastically for cloudy conditions. Because of the low sensitivity of RSIs for blue wavelengths, the spectral response of the RSI for DHI has an error of up to 70 %. Analyzing a variety of parameters, the clearest dependence emerged on $PI = DNI \bullet GHI / DHI^2$, with the Direct Normal Irradiance (DNI) and the Global Horizontal Irradiance (GHI). Therefore, we apply a similar correction as in [Geuder2008] over the spectral parameter *PI*. Figure 14 shows this dependence with the ratio of reference to raw RSI DHI as an ascending blue colored band plotted over *PI*.

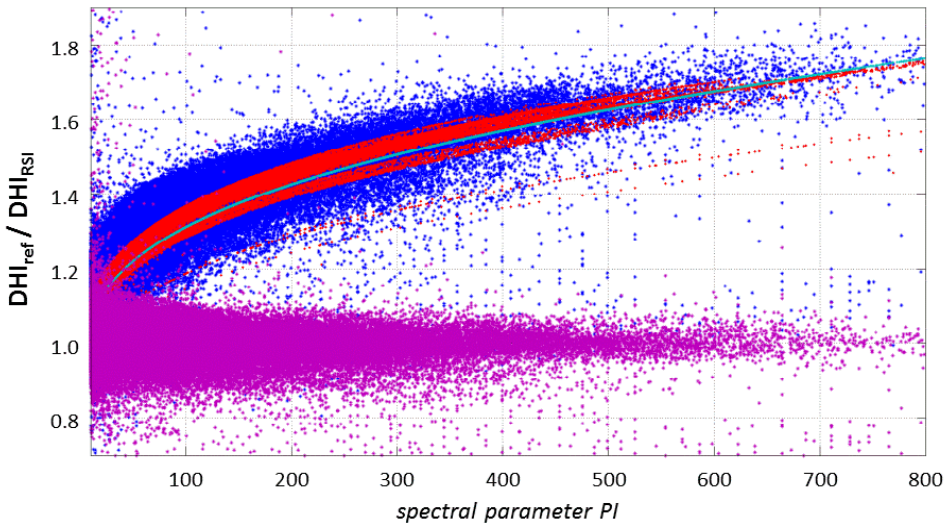

Figure 14: Ratio of DHI values of reference to RSI data before correction (blue) and with applied correction (purple) in dependence on the spectral parameter. The turquoise line shows the spectral PI correction, the red data points include additional varying air mass and/or altitudes.

A further error in the diffuse irradiance response in the order of <5 % can be related to the variation of the air mass in dependence on solar elevation and site altitude. This is accounted in the correction functions with additional terms depending on air mass and site altitude. The full DHI correction (including spectral dependence, air mass and altitude correction) is also depicted in Figure 14. The turquoise line represents the spectral correction function *f(PI)* for a particular airmass and altitude. Its course changes with varying airmass and different site altitudes. This is plotted here with the red data points for an air mass range of 1 to 38 and site altitudes between 0 and 2200 m. The purple band finally refers to the ratio mentioned above but for corrected RSI data and is spread around a value of 1, meaning coincident DHI values.

6.5.2. Correction of Global Horizontal Irradiance

The Global Horizontal Irradiance (or total irradiance) is composed by two components: the direct solar beam and the hemispherical diffuse irradiance originating from the sky. With the impacts on the diffuse component treated yet, the influences presented in the following act merely on the direct component and are therefore applied only on the portion of the Horizontal Direct Beam Irradiance: *BHI = GHI - DHI*.

An important contribution to the RSI's error on the direct component results from angular effects at low solar elevations. Measurements of the response of the LI-COR pyranometer in dependence on the incidence angle of the solar beam yield a characteristic deviation in the order of 10 % (see Figure 15). This effect was yet referred by further authors as the so-called "cat-ear" effect. Estimated reasons for this behavior are the finite size of the diffuser plate, the fact that the curb of the LI-COR housing throws a shadow on parts of the diffuser plate for angles below roughly 10° and increasing specular reflections on the diffusor surface at grazing inci-

dence angles. An angular correction below an apparent sun height of 20° as shown by the green line in Figure 15 is applied to the BHI portion of GHI. Furthermore, the influences of the varying spectrum of the direct solar beam with changing air mass are respected with a similar corresponding correction like at the diffuse component.

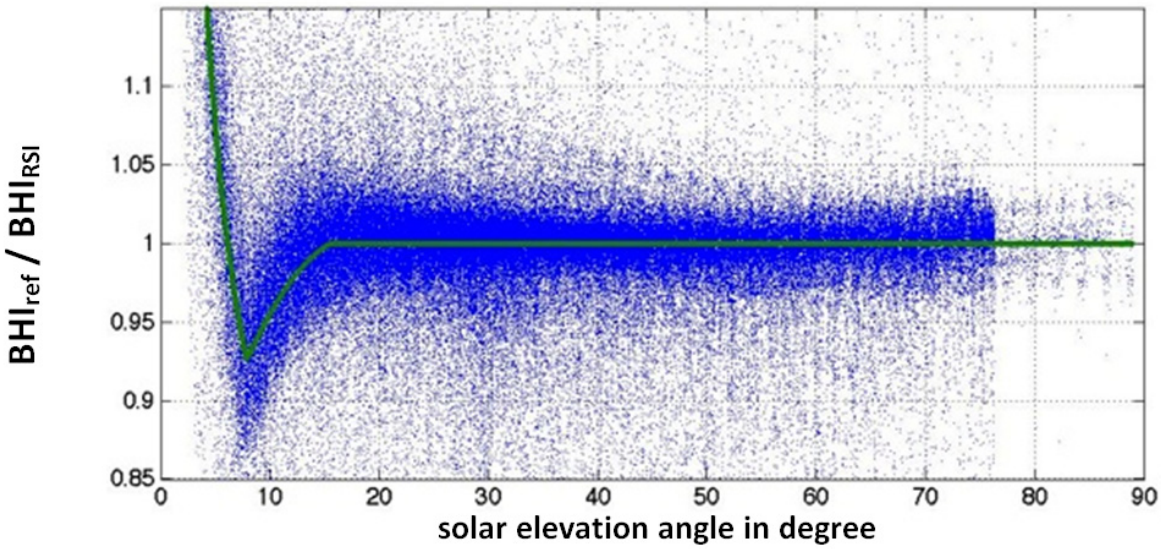

Figure 15: BHI ratio of reference to RSI measurements (blue data points) and corresponding correction function (green line) in dependence on the solar elevation angle, showing the "cat-ear" peak at low solar elevations

6.5.3. Altitude correction for GHI and DHI

After applying the mentioned corrections on the measured global and diffuse irradiances, a dependence on the altitude of the measurement site above mean sea level has been detected for some sensors analyzed and calibrated at some selected sites around Almería with different altitudes. The dependence on the site altitude is presented in Figure 16. This observation has been confirmed with devices which have been installed in other regions and countries aside high-precision instruments at altitudes deviating from the 500 m altitude of the PSA. Therefore an additional correction for site altitude has been derived for the GHI and DHI signal with 500 m of PSA as mean reference altitude.

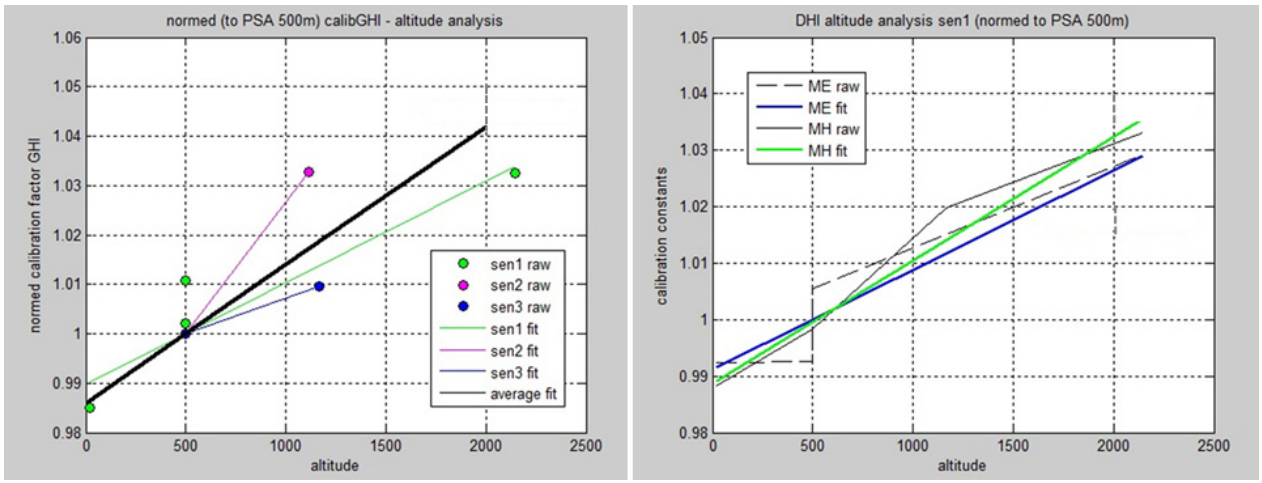

Figure 16: Dependence of the Calibration Factor CF on the altitude above mean sea level for GHI (left) and for DHI (right)

6.5.4. Correction of Direct Normal Irradiance

The DNI is finally calculated from the difference between GHI and DHI divided by the sine of the apparent solar elevation [Michalsky1988]. A final minor linear intensity correction allows fine adjustment of the correction coefficients for each individual LI-COR pyranometer.

As remaining effect, partially deviating branches for morning and afternoon data are stated (as reported also by other authors [Vignola2006]) but not parameterized so far. Slight azimuthal tilts of the sensors due to imperfect installation can be excluded here as cause as it should average out with 39 RSIs. As it refers to absolute deviations in the order of 2 W/m², remaining measurement errors due to temperature effects of the ventilated and corrected reference instruments may cause this deviation.

7. Calibration of RSIs

Up to now, RSIs with continuous rotation are usually equipped with a LI-COR LI-200 pyranometer silicon sensor. They usually come pre-calibrated for global irradiance against an Eppley pyranometer (PSP) by the manufacturer LI-COR with an accuracy of <5 % [LI-COR]. Besides the uncertainty of the pre-calibration, the silicon sensor response is depending mainly on the spectral distribution of the incoming radiation, instrument temperature and the incidence angle. Altogether this may sum up to systematic measurement errors of easily 10 % and more for the instant DNI response (at relevant irradiances) and yield annual sums deviating in the order of 7 % from the true value (usually measurements exceeding the true irradiation). Therefore a thorough calibration of the RSIs for utmost accuracy also for the derived quantities like diffuse and direct irradiance is indispensable. Besides, the stability of the sensor sensitivity needs to be characterized and controlled within the measurement period.

It is exceedingly difficult to obtain a good calibration number for a photodiode based pyranometer when using broadband measurements. This results basically from the responsivity of the photodiode being dependent on the spectral distribution at the time of calibration.

When a photodiode based pyranometer is calibrated over the year and subjected to different solar spectral distributions, one can begin to get a good understanding of the responsivity's dependence on the spectral distribution in addition to obtaining information on the cosine and temperature response.

7.1. Calibration Methods

The calibration of an RSI is crucial for the system performance and more than the calibration of the pyranometer alone. A pre calibration of the commonly used pyranometer in RSIs is carried out by the manufacturer against an Eppley Precision Spectral Pyranometer for 3 to 4 days under daylight conditions. Further calibration efforts are usually performed for the application in RSIs.

Due to the rather narrow and inhomogeneous spectral response of the photodiodes and the combined measurement of DHI and GHI, ISO 9060 cannot be used for the complete specification of RSIs. The existing standards for the calibration of irradiance sensors refer only to the instruments described in ISO 9060. Therefore, only some aspects can be transferred to RSI calibration.

The calibration methods described in ISO 9846 [ISO9846 1993] and ISO 9847 [ISO9847 1992] for pyranometers and in ISO 9059 [ISO9059 1990] for pyrheliometers are based on simultaneous solar irradiance measurements with test and reference instruments recorded with selected instrumentation. Only the annex of ISO 9847 for pyranometers refers to calibrations with artificial light sources. For calibrations using a reference pyrheliometer ([ISO9059 1990], [ISO9846 1993]) at least 10 series consisting of 10 to 20 measurements are taken under specified meteoro-

logical conditions. Preferably, measurements should be taken around solar noon and when DNI is greater than 700 W/m². The angular distance of clouds from the sun has to be greater than 15° for pyrheliometer calibration and >45° for pyranometers. Also, cloud cover should be less than 1/8, the cloud movement has to be considered for the calibration and Linke turbidities should be less than 6. For pyranometer calibrations using a reference pyranometer [ISO9847 1992], the sky conditions are less defined. The calibration interval is adjusted depending on the sky conditions.

Calibration of RSI instruments involves calibration for DNI, DHI and GHI. Due to the spectral response of the instrument it is problematic to calibrate based on only a few series of measurements and under the special conditions defined in ISO 9847 and ISO 9059. This is only possible for thermal sensors due to their homogenous spectral response covering at least 300 nm to 3 µm (>99 % of the ASTM G173 airmass 1.5 DNI spectrum). Preferably, a wide variety of meteorological conditions have to be included in the calibration period and then selected wisely at the calibration process. The accuracy of the calibration generally improves when the conditions during the calibration represent the conditions at the site where the RSI later is operated. In addition to the cloud cover, the influences of aerosols and site altitude on the solar spectrum have to be considered. Calibrations with artificial radiation sources usually lack the variety of irradiation conditions; therefore field calibrations under natural irradiation conditions are preferred.

For all calibration methods it is very important to characterize the spectral dependence of the reference pyranometer to obtain the best estimates of the temperature and cosine responses.

RSI calibrations are performed for example at NREL in Golden, Colorado or by DLR on the Plataforma Solar de Almería (PSA) in Spain. In all of the extensively presented cases, RSIs are operated parallel to thermal irradiance sensors under real sky conditions (see Figure 17 and Figure 18). The duration of this calibration is between several hours and several months, thus providing a data base for the analysis of systematic signal deviations and measurement accuracy. Data quality is analyzed and compared to the reference irradiances.

E.g. on PSA, the precision station is equipped with a first class pyrheliometer mounted on a two axis tracker with a sun sensor (see Figure 17). Secondary standard pyranometers are used for GHI and DHI measurements. The direct GHI measurement is used for the quality check of the measurements by redundancy. The reference instruments at PSA are regularly calibrated by the manufacturers or against a PMO6-cc Absolute Cavity Radiometer and a CMP22 pyranometer to gain utmost accuracy. RSI calibrations are performed according to the different methods that are described in the following sections.

Other methods are possible, too, although they are not described and evaluated here. One not further documented, but promising approach to calibrate a photodiode pyranometer is to establish a reference photodiode pyranometer of the same

model and use the reference pyranometer to calibrate the photodiode based pyranometer under study. The temperature response, cosine response, and spectral response of the reference pyranometer will be similar enough to the pyranometer being calibrated, that a decent calibration number can be obtained. This is especially true if the responsivity is normalized to a reference solar zenith angle, say 45°.

In this manner the degradation rate of the pyranometer might be tracked with more accuracy because much of the spectral response as well as the temperature and cosine response has been taken into account by using the reference pyranometer of the same type. Water vapor and aerosol measurements at the site of interest could then be used to estimate the change in responsivity brought about by changes in the spectral distribution.

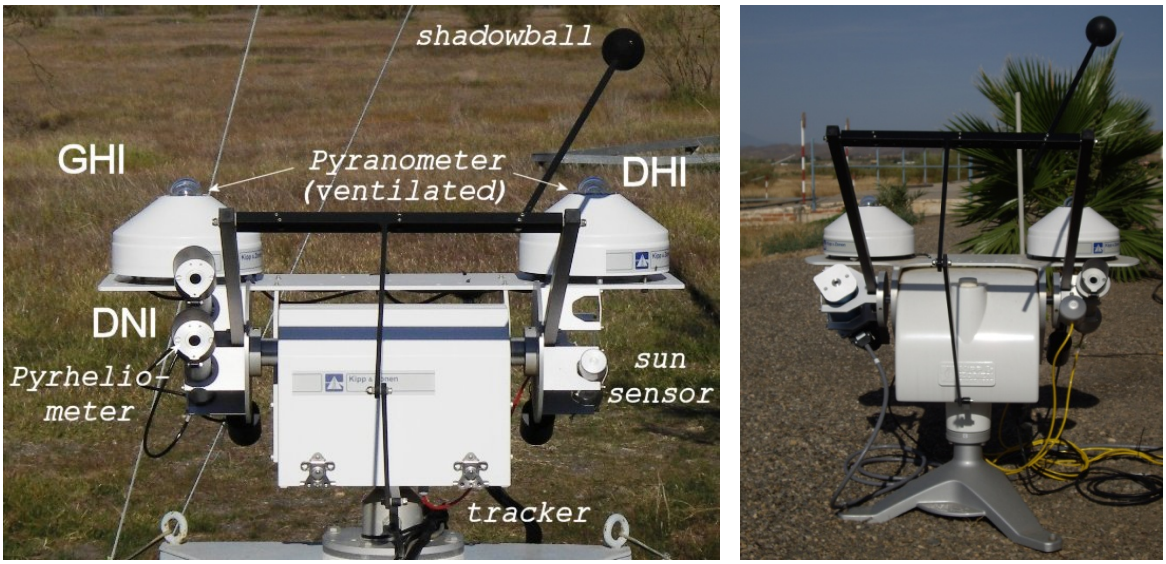

Figure 17: Thermal irradiance measurement sensors (left picture) and Solys 2 tracker with PMO6-cc absolute cavity radiometer (right picture) of DLR at Plataforma Solar de Almería.

Figure 18: RSI calibration mount of DLR at Plataforma Solar de Almería.

7.1.1. Method 1

The constant calibration factor and the diffuse correction are determined by comparing the precise direct normal and diffuse horizontal irradiation to corresponding RSI irradiation data as determined with the LI-COR calibration constant and including correction functions developed by DLR in 2008 [Geuder2008]. The RMS (root mean square) deviation of the 10-minute means for DHI is minimized by variation of the thereby determined diffuse correction. Then the RMS deviation for the DNI is minimized using the constant calibration factor. Irradiation data from the RSI and the DLR station is logged as 60 second averages during the entire calibration process. For calibration, only the relevant operation range of solar thermal power plants is considered with DNI > 300 W/m², GHI > 10 W/m², DHI > 10 W/m² and at sun height angles > 5°. Outliers with deviations of more than 25 % are not included. In order to contain sufficient variation of sky conditions, the measurement interval covers at least two months. Usually two correction factors are defined. An enhanced version with four correction factors based on the same data is also possible [Geuder2010].

7.1.2. Method 2

Another approach for RSI calibration also developed and performed by DLR involves the correction functions presented by Vignola [Vignola2006]. The other aspects are very similar to the ones described in method 1. The subset of data used for the calculation of the calibration factors is slightly different (DNI>250 W/m², outliers defined as deviation of more than 15 %). Three correction factors are defined here. After applying the correction functions, the thus calculated GHI, DNI and DHI are multiplied with a constant respectively. First, the RMS deviation of the 10-minute means for GHI is minimized by variation of the thereby determined GHI calibration

constant. Then the RMS deviation for the DHI and finally that of the DNI is minimized using the corresponding constants.

7.1.3. Method 3

A further method suggested by [Kern2010] uses only GHI data for the calculation of a calibration factor. This allows the calibration of the LICOR sensors without a shading device. Exclusively measurements collected for solar zenith angles between 56.8° and 58.8° are used, collected in intervals with low temporal variation of GHI and low deviation of DNI to its theoretical clear sky value according to [Bird1984].

7.1.4. Method 4

To obtain the correction factors for the corrections described in section 6.5, a calibration method slightly differing to methods 1 and 2 from DLR has been developed by CSP Services: primarily clear sky and clouded sky data points were separated by filtering the high-precision reference DNI with DNI calculated according to the Bird model [Bird1984]. Subsequently, the GHI correction constant is calculated using only clear sky days and DHI using only cloudy days because raw data uncertainty is lowest there. The correction constants are derived by minimizing the RMS deviation with the functional corrections applied. RSI data deviating by more than 40 % from the reference data as well as reference data exceeding their redundancy check by more than 5 % are rejected as outlier.

7.2. Analysis of the necessary duration of an outdoor calibration

The duration of the outdoor calibration has been investigated exemplary for one SMAG/Reichert RSP. The RSI was operated in parallel to DLR's meteorological station as presented for calibration method 1 for 18 months. The data set was used for multiple calibrations of the RSI using different length of the calibration period from 1 day to 6 months. The various calibration results were grouped according to the length of the calibration interval and compared to the calibration based on the complete data set. Separate calibration constants were determined for DNI, GHI and DHI. The result of this analysis is shown in Figure 19 and Figure 20.

In Figure 19 the deviation of the daily, weekly and monthly average of the ratio of the reference DNI and the corrected RSI derived DNI from the corresponding long-term average ratio derived from the complete data set is shown. No significant drift can be seen for DNI. For the corresponding ratios for DHI the variation is more pronounced, especially for the DHI.

In Figure 20 the maximum deviation of the three ratios from their long-term value are shown in dependence of the duration of the calibration period. In the example the maximum deviation of the ratios from the long term mean doesn't improve significantly with the duration of the calibration period if at least 4 weeks of measurements are used. However, this example cannot be used for all weather conditions during the calibration period. This holds even if the calibration is always performed

at the same site and without including questions concerning site specific calibration results. The required duration of the calibration depends on the sky conditions. To be able to guarantee a certain accuracy of the calibration its duration has to be adjusted to the sky conditions. Alternatively the calibration always has to be performed for a longer time as the found 4 weeks (e.g. 2 months).

Further instruments are currently under investigation. Another approach for the selection of the correct calibration duration might be to select or weight the data used for the calibration such, that it always corresponds to the same DNI, DHI and GHI histograms.

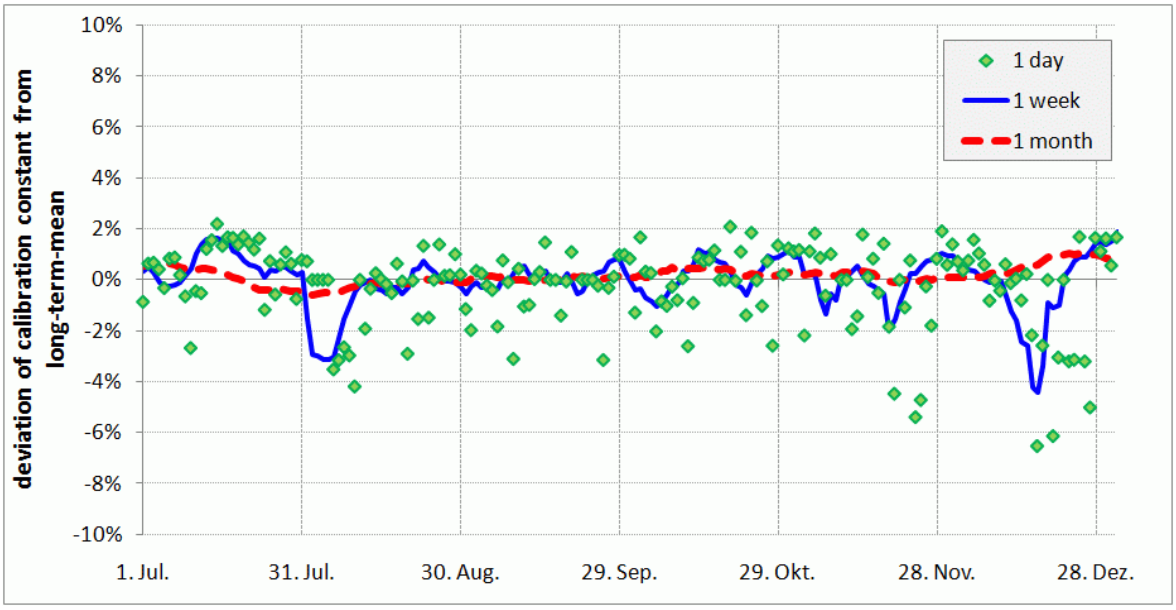

Figure 19: Variation of the average ratio DNI_{corr}/DNI_{ref} for daily, weekly or monthly calibration (as running average) over a period of 18 months

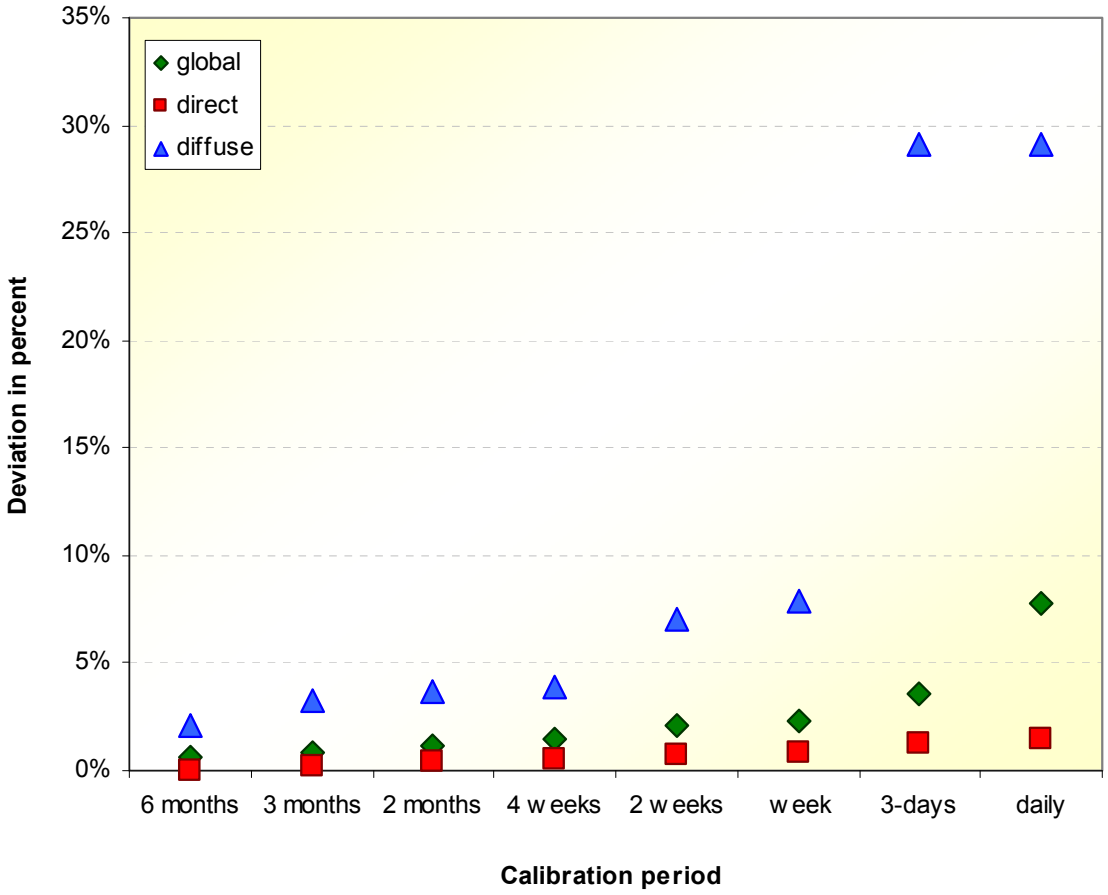

Figure 20: Uncertainty of the derived ratios DNI_{corr}/DNI_{ref} as deviation from its long-term value in dependence of the duration of the calibration period

7.3. Stability of RSI sensor sensitivity and calibration constant

The stability of the LI-COR sensor sensitivity and subsequently the calibration constant is given by the manufacturer to remain within 2 % change per year. With an accuracy of the annual irradiation sum of within 1 %, a sensor drift in this dimension would quickly and systematically exceed the other uncertainties and require soon a re-calibration of the sensor. Within the DLR calibration process (Method 1) Correction Factors *CF* are derived for application with the corrections.

The variation of the Correction Factors was further analyzed for 29 different devices, which were back for re-calibration at DLR after a period between approximately 2 to nearly 4 years, to check the stability of the sensor sensitivity and deduce the necessary or recommended frequency of re-calibration.

Figure 21 presents the absolute values of the Correction Factor of the first and the re-calibration (left side) as well as the relative variation of the *CF* per year (right). Besides one sensor with a change of 3.4 % within one year, all sensors are within the manufacturer-specified range. Indeed this instrument got conspicuous delivering suddenly suspect values; possibly this was caused by an external influence. If such a significant drift is detected with the recalibration, the previous measurements should be recalculated with a temporally interpolated series of calibration

constants in a first approximation unless a reason connected to a certain event can be stated as probable cause for the change of the sensor sensitivity. The measurement error usually remains within the order of the drift plus usual RMSD (root mean square deviation). Nevertheless, the sensor head should be examined and preferably exchanged.

The majority of the analyzed sensors show variations of their *CF* of around and less than 1 %, which remains within the accuracy of the calibration and inclusively within the calibration accuracy of the reference pyrheliometers. The latter were subject to re-calibrations within that time, too. Thus, so far no obvious elevated sensor drift can be stated from the analyzed sensors.

However, no exact quantitative statement of the drift per year can be deduced from the result of the here analyzed instruments. The proper readings of the sensor should be checked at regular inspection visits and the device re-calibrated at regular intervals of around 2 years.

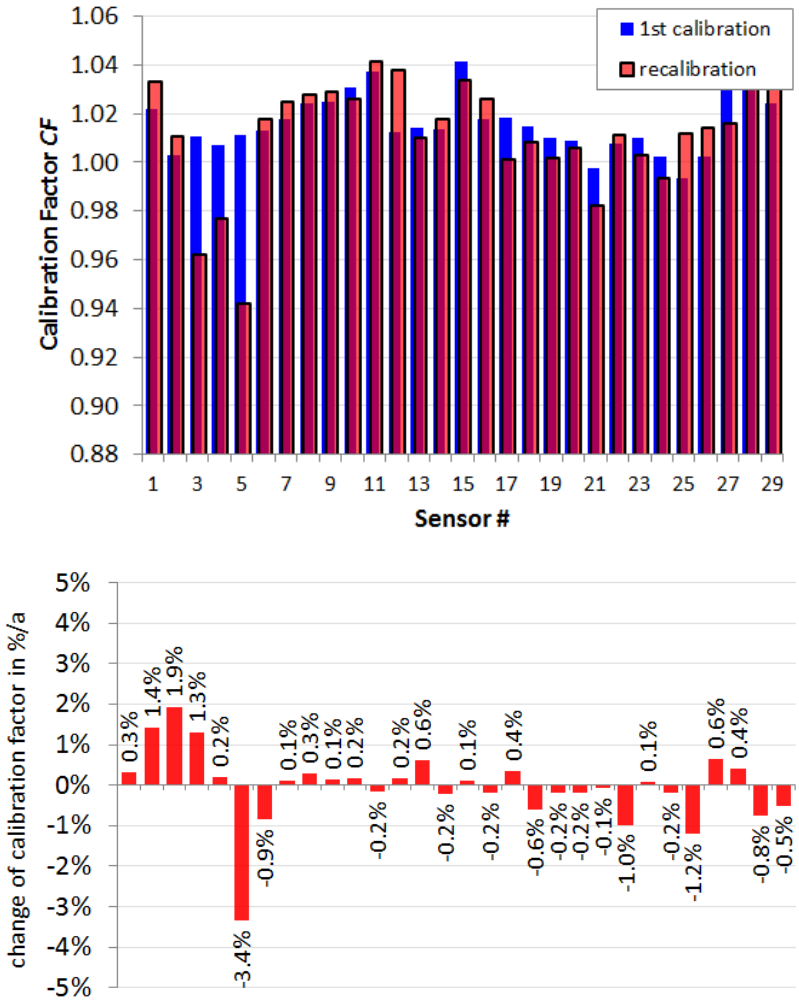

Figure 21: Variation of the RSI Correction Factor CF as detected on re-calibration of 9 sensors after a period of between 2 to 3¾ years: absolute values (up) and corresponding relative variation per year (down).

8. Case studies of RSI accuracy

8.1. Resulting Performance of DLR 2008 Correction Functions (method 1)

The quality of the correction algorithm finally is analyzed on its capability to reproduce the reference irradiation. Therefore the running values of the deviation between the reference and the corrected data were compared as well as integral measures like mean bias, root mean square deviation (RMSD), standard deviation, the correlation coefficient and the total irradiation sum within each comparative period.

In Figure 22, the deviation between the corrected RSI values and the reference data is plotted against the intensity of the reference irradiation. To see the improvement by the correction, also the original response ("raw data" with bright color) is shown. The shown data set here includes data of all 23 analyzed RSIs (for this study Reichert/SMAG RSPs were used). The distribution of the corrected global data (left graph) is mainly spread within a range from -20 to 30 W/m² over its entire intensity at an RMSD of ±10.2 W/m². The original global response of the LI-COR on the contrary clearly underestimates the true irradiation with increasing values until 40 W/m² at over 800 W/m² and an RMSD of 13.7 W/m².

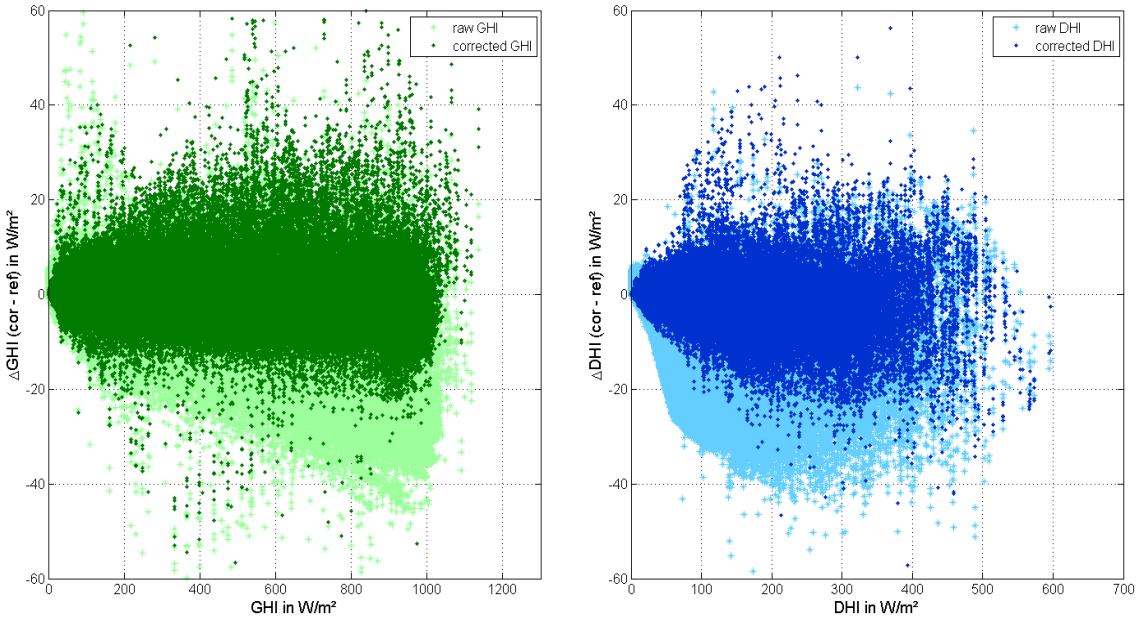

Figure 22: Deviation of the corrected global (left graph) and diffuse RSI values (right graph) to its corresponding reference irradiation values, including the combined data of all 23 analyzed RSIs.

The deviation characteristic of the corrected diffuse irradiation (right graph of Figure 22) represents a spread increasing to values of around ±20 W/m² at medium intensities of 250 W/m². The deviation of the original DHI data reaches also values down to -40 W/m² however yet at far lower intensities. The higher original RMSD (compared to GHI) of 16.3 W/m² is reduced here to a value of 6.1 W/m².

The deviation of direct normal irradiation is shown in Figure 23: the distribution of the corrected data is spread mainly within a range of ±25 W/m² with deviations of several data points until 100 W/m², single values even more; its absolute RMSD is 17.3 W/m². The uncorrected DNI on the contrary shows a clear overestimation of the RSI of up to 150 W/m², mainly at intensities around 550 W/m². This is reflected in an absolute RMSD value of 53.7 W/m².

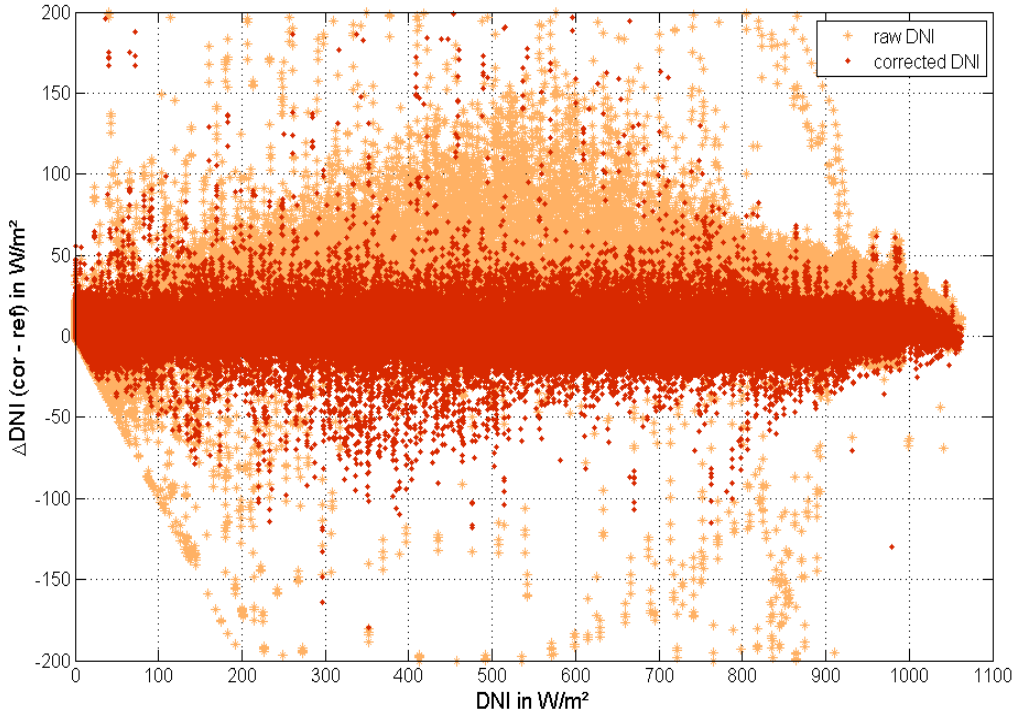

Figure 23: Deviation of the corrected RSI direct normal irradiation values to reference DNI including the combined data of the 23 analyzed RSIs

However, these denoted RMSD values refer to the complete set of 23 different sensors and represent the accuracy for the determination of the correction functions. They are not representative for the resulting accuracy reachable with one particular RSI. To get the accuracy for one device, the MBE and the RMSD has to be determined for all devices separately and then averaged. These values are listed in Table 5 for uncorrected data as well as corrected data resulting from this and the former correction algorithm. The "ref" column denotes the accuracy of the reference data via the consistency of its three measured components. Here only data sets with direct irradiation beyond 200 W/m² were evaluated as usually very low DNI is not used by concentrating solar power plants.

The mean bias of the uncorrected raw DNI data shows a value of 25 W/m² as the average of the 23 sensors, several of them however differed by even more than 37 W/m². Maximum values for GHI and DHI were around -17 W/m² and -21 W/m² with average values of -10 W/m² and -17 W/m², respectively. Both correction algorithms reduce these values considerably to around the accuracy of the reference data of 1.0 W/m², most notably the variation spread. The RMSD decreases from 14 W/m² to 8 W/m² for global irradiation with the here developed corrections, from

19 W/m^2 to 5 W/m² for diffuse and from 33 W/m^2 to below 15 W/m² for direct normal irradiation. The RMSD is illustrated in Figure 24 and Figure 25 separately for the individual RSI. Thus, a relative standard deviation of the RSI data of 3 % is reached for Direct Normal Irradiation beyond 200 W/m² and 2.4 % for DNI beyond 300 W/m², taking into account an inaccuracy of 1.5 % of the reference data. Concentrating Solar Power Plants are usually operative beyond these irradiation limits.

Table 5: Average values of Mean Bias, Root Mean Square Deviation and relative deviation of the irradiation sum from the 23 RSI data sets: for the uncorrected raw data and for corrected data (along the two DLR algorithms), as well as the accuracy of the reference data set ("ref").

	GHI			**DHI**			**DNI**			**ref**	*unit*
	uncor	*cor$_{old}$*	*cor$_{new}$*	*uncor*	*cor$_{old}$*	*cor$_{new}$*	*uncor*	*cor$_{old}$*	*cor$_{new}$*		
average MB	-10.3	-0.3	0.3	-17.3	-0.3	-0.4	24.6	-1.4	1.0	1.0	*W/m²*
± spread	*±4.0*	*±3.9*	*±1.3*	*±1.6*	*±2.3*	*±0.7*	*±10.5*	*±1.0*	*±0.5*	*±3.9*	
RMSD	14.2	10.4	7.6	18.9	7.8	4.5	33.3	15.4	14.5	5.3	*W/m²*
Sum	-1.9%	-0.1%	0.0%	-14.2 %	-0.5%	-0.4%	3.5%	-0.2%	0.1%	0.2%	

Without corrections, the sum of the measured uncorrected irradiation is 2 % too low for global irradiation, 14 % too low for diffuse radiation and more than 3 % too high for DNI. By applying the correction formulas, the error falls below the uncertainty of the reference data.

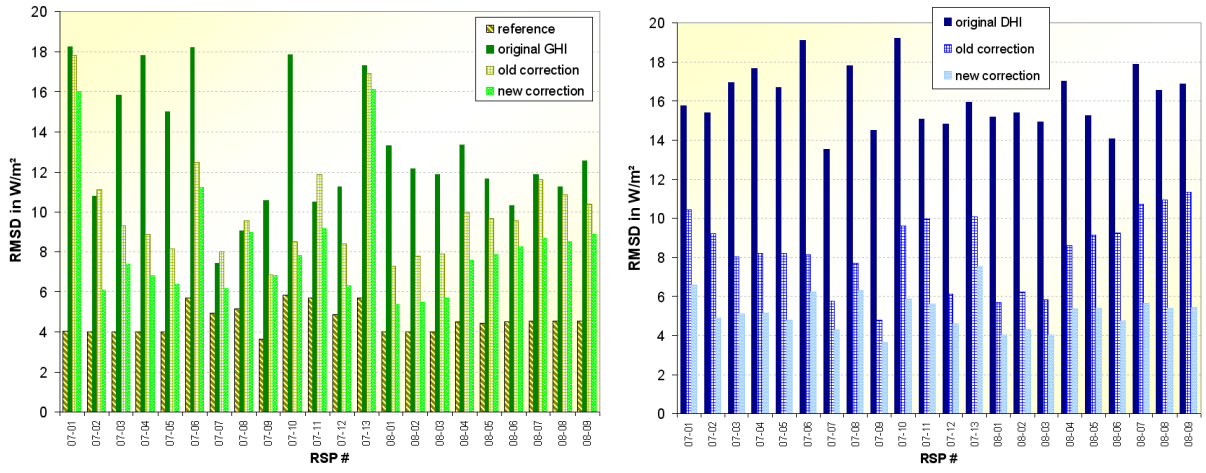

Figure 24: RMSD of GHI (right) and DHI (left) of uncorrected data as well as for both corrections (and reference data accuracy).

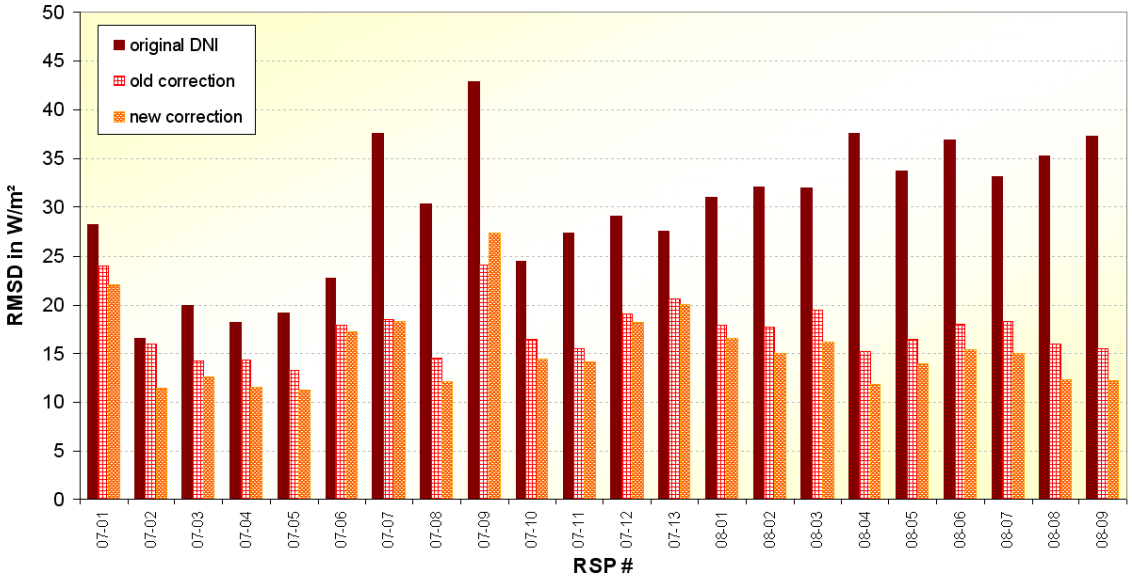

Figure 25: RMSD of DNI from uncorrected data as well as for both corrections

The correction algorithm was developed for Rotating Shadowband Irradiometers, which additionally are measuring their sensor temperature. The correctional functions were developed on the basis of data sets from 23 different RSIs over a period of an entire year. Parameters for the correctional functions are sensor temperature, ambient air temperature, the pressure-corrected air mass factor, solar elevation angle and a particular spectral parameter, which is calculated from the intensities of the three irradiation components, i.e. global, diffuse and direct. By means of a thorough re-calibration of the RSI, two sensor-specific constant correction factors are determined separately for global and diffuse irradiation. The correction algorithm finally succeeds to reduce the root mean square deviation of the acquired direct normal irradiation from more than 30 W/m² to below 15 W/m². This reduces the inaccuracy of acquired DNI data for solar resource assessment for concentrating solar power plants to values below 2.5 % at comparatively low installation and maintenance costs, avoiding the unacceptable soiling susceptibility of a pyrheliometer. Future investigations will focus on an exact adjustment of the algorithms to different site altitudes.

8.2. Comparison of different Correction and Calibration Methods

The correction algorithms of [Vignola2006] and [Geuder2008] as well as the here presented enhanced corrections have been selected for comparison, each with its corresponding usual calibration. Algorithm [Vignola2006] is currently used with the two calibration methods 2 and 3 and is therefore examined here with both calibrations. Including the analysis of uncorrected raw data (using LI-COR calibration), finally five cases are compared: (1) the raw uncorrected data; (2) the new enhanced algorithm from section 6.5, called CSPS2011; (3) algorithm [Geuder2008] with notation DLR2008; (4) algorithm [Vignola2006] with calibration method 3 using one single calibration constant, denoted US-1, and finally (5) algorithm [Vigno-

la2006] with application of calibration method 2 with three separate calibration constants, called US-3. Correction [King1997] without correction for DHI and DNI is not considered here nor other algorithms as [Alados1995] because no actual utilization is known at the moment.

The corrected RSI irradiances are analyzed for their coincidence with instantaneous values by examination of their RMSD to the reference data in 10 min time resolution as well as regarding the bias of the data set by evaluating the relative measurement period sum. The calculations are performed for GHI, DHI and DNI. The data of 39 RSIs are included in the analysis to derive statistically sound mean values. The evaluation yields also information on the worst cases from potential bad devices by regarding the extreme values. The largest part of the dataset has been collected on PSA, but also data from four further sites in different climate zones and at different altitudes is used. The mean measurement period of most RSIs was approximately 2 months. However, to eliminate possible seasonal effects, another comparison has been performed with data of one particular RSI from a period of more than 2 years.

8.2.1. Analysis of instantaneous irradiance values (10 min time resolution)

The RMSD for the five analyzed cases is plotted in Figure 26: the raw uncorrected DNI deviates at average of the 39 RSIs 32 W/m² from precise measurements but with a wide spread of individual instruments with mean deviations of between 15 and 57 W/m² depending on the quality of the manufacturer calibration.

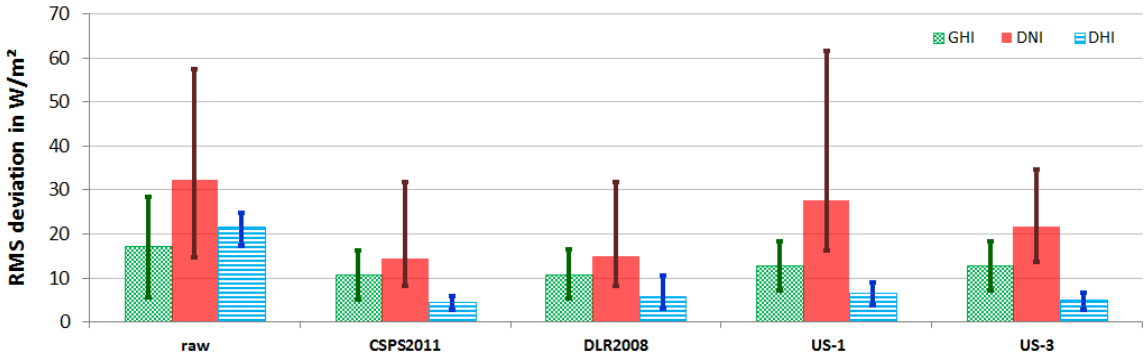

Figure 26: Maximum, mean and minimum RMSD of irradiance values with time resolution of 10 min from 39 RSIs compared to high-precision thermopile sensors. Data sets for uncorrected raw values as well as for four different corrections are analyzed.

The average RMSD value for GHI for the 39 RSIs is 17 W/m² within a range from 6 to 28 W/m² for individual devices. For DHI, the average RMSD is 21 W/m² with a variation within 17 and 25 W/m². Using corrections US-1 with only one calibration constant derived for GHI achieves to reduce the RMSD for GHI and DHI and to a minor extend also for DNI, but this combination of corrections and calibration shows the least capacity to improve RSI data. It even may worsen DNI under adverse circumstances. Notably better yet behaves correction US-3 which yields a reduction of the average RMSD for DNI to 22 W/m² in a range from 14 to 35 W/m²

at mean. The RMSD for DHI reduces to 5 W/m² and to 13 W/m² for GHI like at US-1. DLR2008 corrections achieve to lower the RMSD of DNI further down to at average 15 W/m² with a spread of between 8 and 32 W/m², the RMSD for GHI at average to 11 W/m² (5 – 16 W/m²) and DHI to 6 W/m², slightly worse than the DHI in the US-3 case. The best performance yield the CSPS2011 corrections and calibration with an RMS deviation for DNI of 14 W/m² (8 – 31 W/m²), 10 W/m² (5 – 16 W/m²) for GHI and 4 W/m² for DHI.

8.2.2. Bias analysis with comparison of annual sums

The evaluation of the relative annual sums yields the same order of appropriateness (Figure 27). The deviation of the measured annual DNI with an RSI without any corrections was detected to be within 0 % to 7 % overestimated with an average of 3.3 %. The GHI on the contrary lies within correct results and 6 % underestimation. The annual DHI is underestimated by 11 to 20 % mainly due to the low sensitivity of the LI-COR sensor at short wavelengths. The corrections and method US-1 yields DNI and DHI annual sum at average to 2 % (GHI 1 %); however, individual RSIs worsen the so corrected result with a deviation of the annual DNI of up to 10 %. Using three calibration constants as in US-3 reduces the maximal deviation of the annual sum to 4 % for DNI (3 % GHI) with an average deviation of 1 %. Annual DHI is determined nearly perfect with US-3.

The DLR2008 on the contrary yields a worse performance for annual DHI values with 2 % underestimation at average and up to 6 % at maximum, but delivers the DNI sum with an underestimation of 0.5 % at average and 1.5 % maximum. The results for GHI are nearly identical with DNI values. The CSPS2011 corrections yield annual deviations of less than 0.5 % for all irradiation components and less than 1.5 % maximal underestimation at GHI, lower even for DNI and DHI.

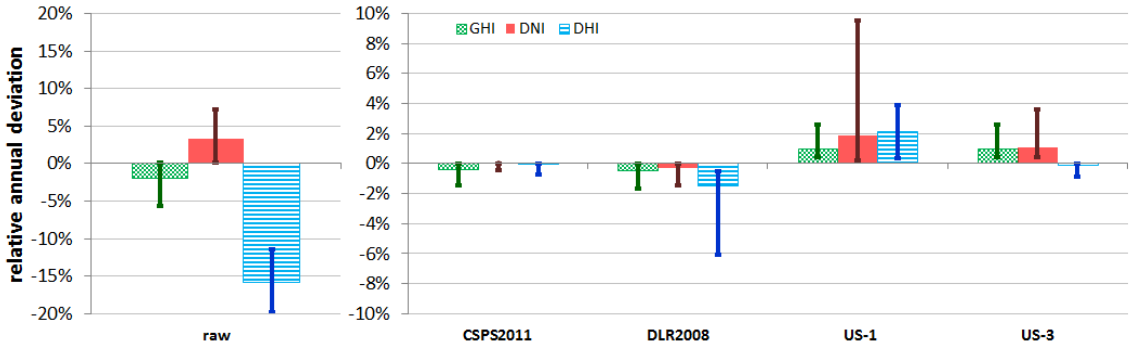

Figure 27: Relative deviation of annual irradiation as acquired by RSIs compared to high-precision reference measurements with (right) and without (left) data correction (at differing scales)

Variations of the calibration period with seasonal changes have not shown crucial changes as long as the duration of the calibration was in the order of at least one month. Additionally, no crucial changes have been detected with application of the CSPS2011 corrections for relocations of RSIs to different sites or altitudes.

8.2.3. Summary of the comparison of different correction functions and calibration methods

The use of corrections and RSI specific calibration improves the RSI performance significantly. Correction algorithms and calibration methods for RSIs were compared. "CSPS2011" and "DLR2008" archive similar results for DNI and GHI, but "DLR2008"performs worse for DHI. For DHI "CSPS2011" and "US-3" perform similarly, but slightly higher deviations are found for GHI and DNI. However, these deviations might be partially explained by the fact that a significant part of the used data was measured at PSA and that CSPS2011 and DLR corrections were developed with other data from the same site.

The methods with two, three or four calibration factors deliver a noticeably better performance than methods with only one calibration factor. The use of correction [Vignola2006] with only one calibration function reaches the lowest accuracy. This is the drawback of the corresponding cheaper calibration method.

8.3. Site dependence of instrument and calibration accuracy - case study in UAE

Five MDI stations were installed for several weeks jointly at one site in UAE to perform parallel contemporaneous measurements aside a high-precision equipment with the aim to evaluate the accuracy of their DNI measurements (see Figure 28). Measurement accuracy was deduced by DLR from calibrations and corrections derived under Spanish climate conditions and need to be proved how they perform under significantly differing climate conditions. In total, six different RSIs were investigated within the period of approximately one year, daily cleaning of the sensors secured.

Figure 28: Contemporaneous and parallel irradiation measurements with five RSIs (on the right) and one station with thermal instruments on a solar tracker (left) at one location in UAE.

Separate measurement campaigns were performed in summer and winter to account for possible influences due to seasonal variations and naturally varying irradiance intensities: During summer months, relatively diffuse skies prevail due to high aerosol loads. They yield mean DNI intensities around 500 to 600 W/m² at ambient temperatures reaching 50°C. In the winter months, the mean DNI intensity is around 800 and 900 W/m² at around 20°C.

The corrected irradiation data of the different RSIs were compared to the values from the corresponding precise instrument with respect to the instantaneous irradiance intensity (10-min time resolution) as well as to daily and annual irradiation sums.

8.3.1. Comparison of instantaneous direct solar beam irradiance intensities

The irradiance values of the RSIs are distributed around the values of the reference within a band of at average approximately ±20 W/m². The DNI distributions of the individual RSIs however are not completely symmetric around the reference values but show a slight device-specific non-linearity with deviations in the order of maximal 2 % within the relevant DNI range. Some RSIs are underestimating slightly low DNI intensities and overestimating high intensities or vice versa. Similar characteristics were also detected in the calibration data of the corresponding RSIs. They refer to intrinsic differences among the individual silicon sensors which are not treated using uniform corrections for all sensors. In its mean, they usually level out within the range of effective intensities with merely a small impact on the irradiation sum – as long as a similar distribution frequency of irradiance intensities acts upon the sensor as during the calibration.

Furthermore, remaining deviations among different RSIs and the UAE reference may originate to a certain amount also from the calibration process on Plataforma Solar de Almería (PSA). The participating RSIs were calibrated at different times against partially different pyrheliometers, which themselves were calibrated meanwhile at Kipp&Zonen with a remaining uncertainty of 1.1 %.

The RMSD of the RSIs analyzed in UAE remain normally within 10 to 13 W/m² or 2.4 % to 2.8 % (for DNI values over 200 W/m²) and thus within the stated accuracy for the current irradiance. Nevertheless, to overcome the stated device-specific deviations of the RSI measurements, an additional correction was applied to the DNI measurements in UAE to correct the non-linearity and remaining leveling in the DNI response of the RSIs. The RMSD correspondingly improve to within 10 W/m² or approximately 0.2 % better. The remaining signal deviation of the six analyzed RSIs is plotted in Figure 29 as absolute value and in Figure 30 as relative value. As the values for relative deviations naturally increase steadily towards smaller irradiance intensities, irradiances below 200 W/m² were not accounted in percentile accuracy statements as they are usually irrelevant for Concentrating Solar Power applications. For DNI intensities over 300 W/m², RMS accuracy is within 2 %.

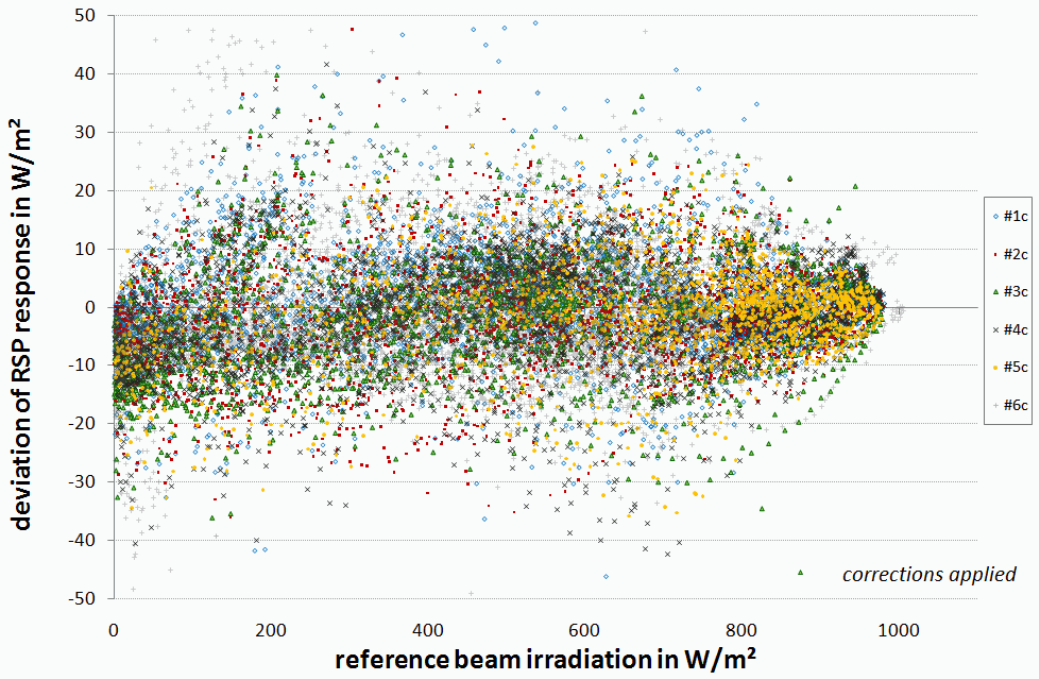

Figure 29: Absolute deviation of the RSI response of six analyzed sensors from the reference after application of additional corrections, in dependence on the reference signal.

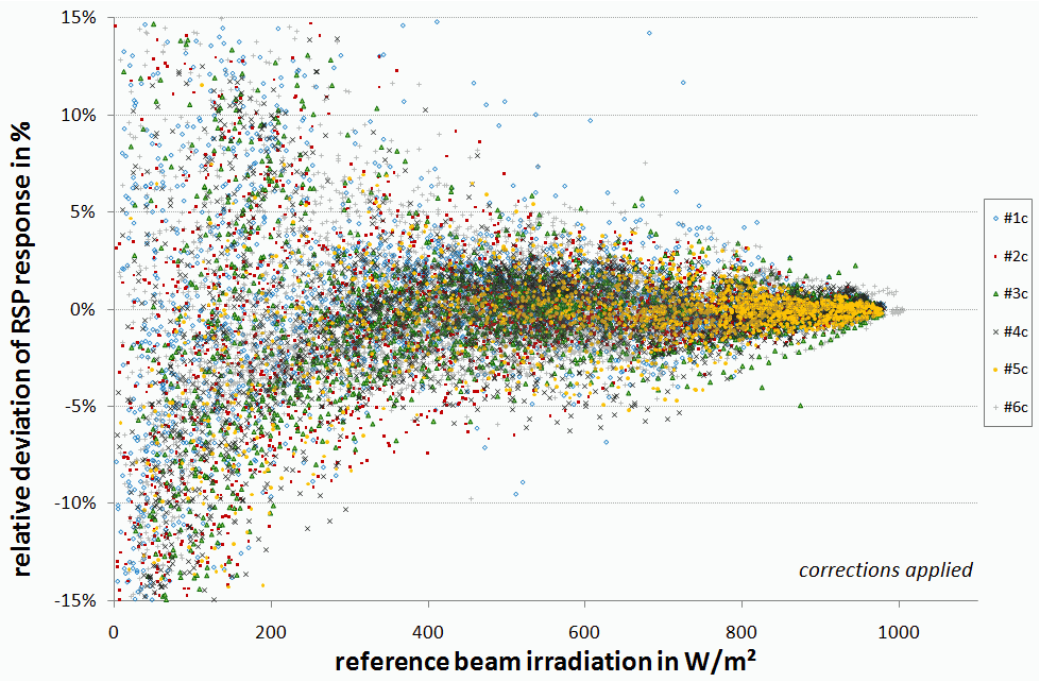

Figure 30: Relative deviation of the RSI response of six analyzed sensors from the reference after application of additional corrections, in dependence on the reference signal.

8.3.2. Impact on and accuracy of daily and annual DNI sums

More important for solar resource assessment is usually the exact determination of the available energy amount and therefore the irradiation sum than a proper measurement of instantaneous irradiance. For evaluation, the deviations of the daily DNI

sums were monitored and the sum over the complete measurement campaign analyzed. Finally, the results were transferred to the annual value.

Figure 31 shows the absolute deviation of the daily DNI sum of the RSIs from the reference for two measurement campaigns in summer 2009 and winter 2009/2010. Figure 32 presents analogically two further parallel measurements of RSIs #1 and #6 in February 2010 and summer 2010. The comparison was performed for all RSI data with and without the additional corrections (notation "c" after the RSI number for data with applied additional corrections). In UAE, mean values of the daily irradiation of around 5.5 kWh/m²d are reached.

The deviations are at slightly different levels for each RSI and follow a certain similar pattern caused by the current weather conditions and to some extend the actual soiling state of the sensors. The coincidence between RSI and reference is usually better with the additional corrections applied and seems to be slightly lower in the winter than in the summer months. The RMSD of the analyzed RSIs is within 0.04 and 0.11 kWh/m²d (usually 1 to 2 %); maximal deviations reach approximately 0.2 kWh/m²d under extreme conditions (around 4 %).

In the winter time, the air temperature was falling frequently below the dew point temperature, causing formation of dew also in the arid climate of the desert in UAE. Whereas both pyranometers are ventilated to suppress the formation of dew on the devices, no ventilation device for the pyrheliometer exists. Therefore sometimes dew is settling on the pyrheliometer cover in the morning hours around sunrise, causing reduced DNI measurements of the reference sensor until it is cleaned and/or the dew is evaporated again due to rising temperature. Dust may be captured by the dew and remain on the cover glass after evaporation, causing a reduced signal due to soiling. The dew effect was detected to different time extensions (20 minutes to slightly over one hour) on approximately 50 days in winter 2009/2010. The reduced DNI measurement from the pyrheliometer within that time yields a reduced daily sum in the same order of magnitude. The incidences are plotted in the winter graphs as thick gray line.

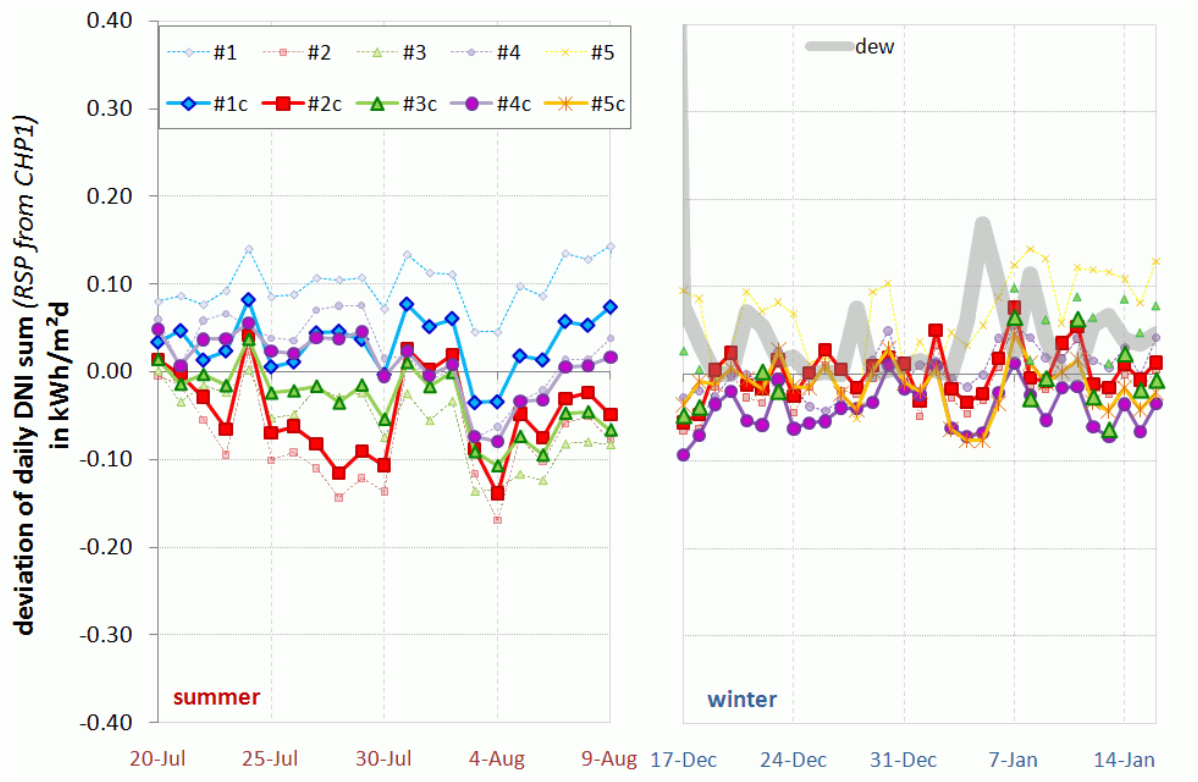

Figure 31: Deviation of the daily DNI as determined by the RSIs with and without additional corrections from the reference value for two measurement periods in summer 2009 and winter 2009/2010.

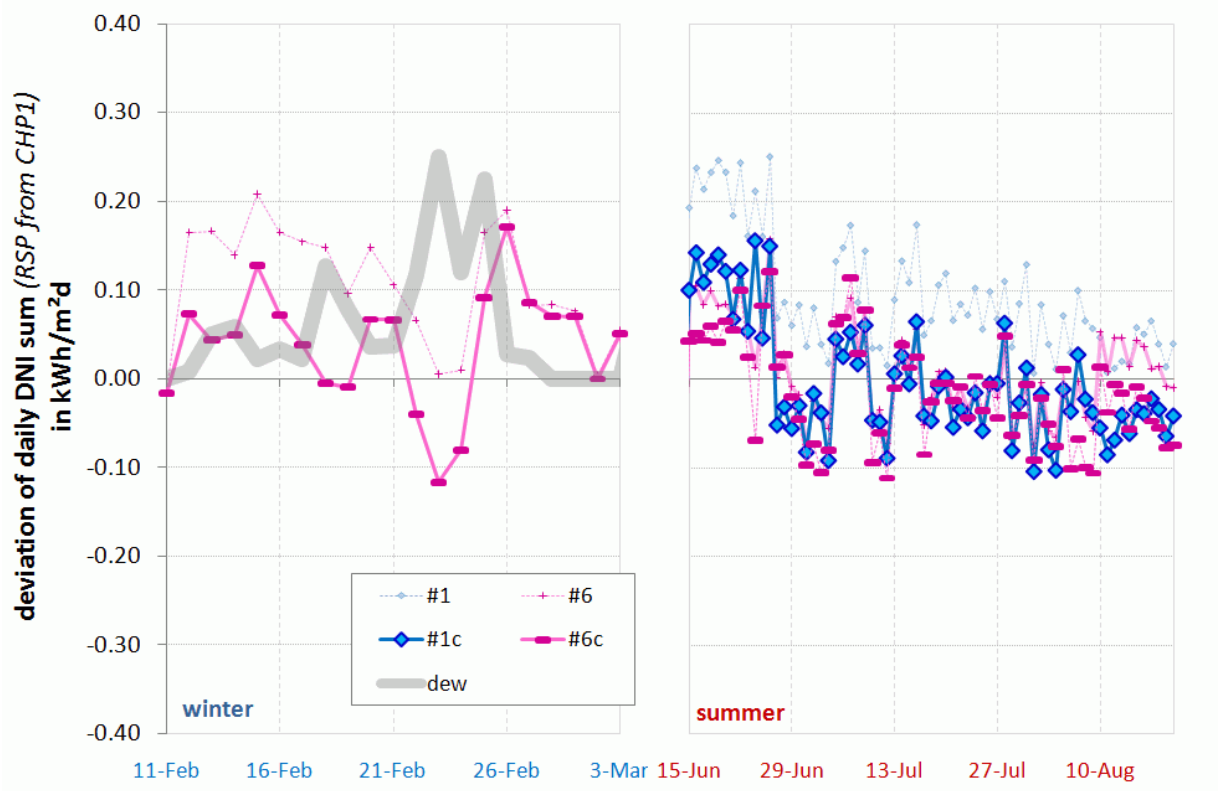

Figure 32: Deviation of the daily DNI as determined by the RSIs #1 and #6 with and without additional corrections from the reference value for two measurement periods in winter and summer 2010.

The detailed RMSD of the individual RSIs are listed in Table 6 for the data including the additional corrections (notation "c") or without (notation "-"). The application of the corrections reduces the RMSD for most devices. Furthermore, also the deviation of the DNI sum over the total period of parallel measurements is given in Table 6. Periods, where apparently dew was detected on the reference sensor, were filtered out. The coincidence of the DNI sum within the whole period for the data without corrections is in the order of 1 % and below with the exception of RSI #1 with a deviation of 2.2 %. With application of the additional corrections, the deviations between the DNI sum detected by the RSIs and the reference were reduced to within ±0.5 %.

To determine the resulting variation of the annual sum when applying the corrections, the corresponding intensity frequency distribution needs to be accounted with the corrections. The results are listed for all analyzed RSIs in the last line of Table 6. The resulting DNI sums of the RSIs subsequently fit within 1.5 % to the value of the precise reference sensor which thus is similar to the accuracy of pyrheliometers.

Table 6: Accuracy of the DNI sum from RSI measurements compared to the reference with (lines "c") and without (lines "-") application of the additional corrections.

RSI #		1	2	3	4	5	6	*unit*
RMS deviation of daily sum	-	0.11	0.06	0.06	0.04	0.08	0.08	*kWh/m²d*
	c	0.06	0.05	0.04	0.04	0.03	0.06	
deviation of period sum	-	+2.2	-0.7	-0.3	+0.3	+1.2	0.7	*%*
	c	+0.2	-0.3	-0.5	-0.4	-0.3	0.0	
variation of annual sum		-1.4	+0.5	-0.2	-0.6	-1.0	-0.9	*%*

8.4. Measurement campaign in Payerne

Currently MeteoSwiss is performing intercomparisons of three different RSIs (twice each) and various Delta-T SPN1 in Payerne, Switzerland, in the framework of the COST Action ES1002 WIRE [Dubis2014]. The investigated RSIs are the RSR2 (Irradiance), the RSP (SolarMillennium/Reichert GmbH) with DLR corrections and the Twin RSI (CSP Services, [Geuder2012]) (Figure 33). Final results are expected for 2014. The reference for the intercomparisons is represented by MeteoSwiss' Baseline Surface Radiation Network (BSRN) data.

Figure 33: Test instruments during the measurement campaign in Payerne (Photo: Meteoswiss).

8.5. Discussion of remaining RSI data uncertainty after calibration and correction

Currently the uncertainty estimations for RSIs basically rely on case studies as presented in the previous chapters. An uncertainty analysis for silicon photodiode based RSIs following GUM is presented in [Stoffel2010]. For subhourly DNI the estimated combined standard uncertainty is calculated as 2.38 % (coverage factor k = 1). A more detailed analysis will be carried out in the framework of IEA SHC task 46.

The remaining data uncertainty after application of a correction and calibration is discussed exemplarily. In this example, the correction developed by [Geuder2008] and the above described calibration are applied. However, the other corrections behave similar.

Figure 34 shows a data set collected during the calibration of RSP 4G-09-18 in 2010 using the first of the described calibration approaches. The ratio of DNI_{CH1} measured with the CH1 pyrheliometer and DNI_{RSP} measured with the RSP is plotted vs. time. The reference DNI_{CH1} is also plotted using the right ordinate. The average of the ratio DNI_{CH1}/DNI_{RSP} for all data points within the calibration period of 2 months is 1.0011. It is depicted as the dark green line in Figure 34. The standard deviation of its distribution yields a value of 0.03 and is enclosing the average value and shown with the light green dashed lines. The reference measurements are estimat-

ed to reach an accuracy of usually around 1 % with an uncertainty of its absolute calibration level of approximately 0.5 %.

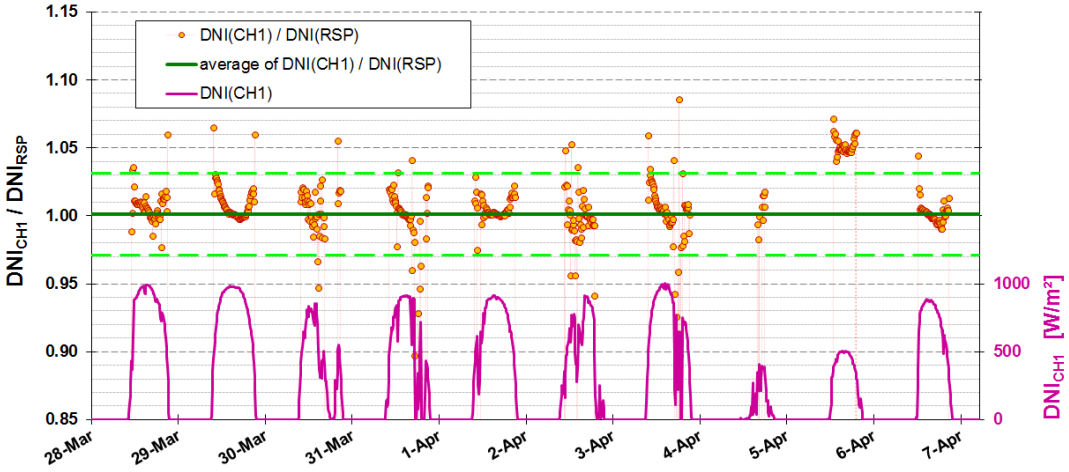

Figure 34: Exemplary data set for an RSI calibration using method 1 (DLR's correction functions [Geuder2008]) from 2010. The ratio of DNICH1 measured with the CH1 pyrheliometer and DNI_{RSP} measured with the RSP plotted vs. the time (average of ratio ± standard deviation in green). Also shown at the bottom is the reference DNI(CH1) (purple) for each 10 min measurement of the RSP plotted vs. time.

The DNI ratio varies noticeably between adjacent data points and from day to day. While rather systematic air mass dependent deviations can be observed for clear sky days, the deviations are more scattered for cloudy days. Also deviations of the whole daily level can be seen for example between day April 6th and day March 30th. This can be explained by the high aerosol load on April 6th (aerosol optical depth (AOD) of 0.5 for 500 nm) while a low aerosol load (0.1, 500 nm) was measured on March 30th. The AOD measurements were obtained with a CIMEL CE-318N EBS9 sun photometer [Holben1998] installed next to the calibration facility.

The example illustrates that RSI measurements of DNI match precise sensors in an acceptable way for many applications. However, it also shows the limits of the corrections and calibration procedure. The dependence of the photodiode response on the AOD and on the presence of clouds is evident. It is a result of the inhomogeneous spectral response of the LI-COR sensor used in most RSIs and has to be considered when using the RSIs under sky conditions differing from those during the calibration period. The exemplary observations of measured RSI data confirm the results of possible deviations derived by [Myers2011] via theoretical investigations with radiative transfer models. They also suggest that it is possible to further increase the accuracy of RSI sensors if additional input parameters such as the AOD are included. However, measurement campaigns with several RSIs in different climate zones also confirmed a general applicability of the calibration and instrument transfer for solar resource studies [Geuder2010] if the annual sum is more important than instantaneous irradiance accuracy.

9. In situ measurement conditions for meteorological stations for solar energy applications

Solar energy projects often rely on large flat areas far from sources of air pollution like industry or cities. Therefore interesting sites are most commonly in remote areas. The measurement of DNI, during project development therefore relies on automatic systems, which require low maintenance effort. Cleaning of sensors must be reduced to a minimum to reduce costs, while significant loss of accuracy in measurements cannot be tolerated. The following chapter focuses on the impact of natural soiling on RSI and Pyrheliometer systems for DNI measurements.

9.1. Analysis of RSI data during cleaning

This section is about the analysis of RSI irradiation measurements during the event of cleaning, thus to see the impact of soiling in a real environment. For the soiling analysis the date and time of cleaning events were logged. After a period of almost one year, the minute data of the cleaning events were analyzed. The observed station was located in an arid area with sandy ground and low bushes. Cleaning was done at irregular intervals between three to 26 days. An accurate analysis of the impact of soiling can only be made at clear sky conditions when direct radiation is stable. Otherwise the dynamic variation of direct irradiation measurements is significantly higher than the impact of soiling. Due to this fact, only four out of 20 cleaning events could be used for the analysis. All other cleaning were made under sky conditions not stable enough for evaluation. Figure 35 shows the corresponding measurement curves, based on data recorded at one minute intervals. Each curve shows a sudden drop in global horizontal irradiation (GHI) during the event of cleaning. The difference of measurement levels before and after the cleaning event states the impact of soiling. As solar irradiation is only stable at solar noon time, trend lines showing the trend of the cleaned sensor have been inserted allowing the comparison of measurements before and after cleaning. Five minute values were used to compare the trend line with the measured values before the cleaning event. The average of the difference shows the soiling of the sensor. Cleaning was done at arbitrary times during the day. Depending on the time of the cleaning event, the solar irradiation is either rising (morning) or falling with proceeding time (afternoon).

Figure 35: measurement curves at cleaning events from four occurrences (a–d)

Table 7 shows the resulting impact of soiling at the four events of cleaning. The occurrences of cleaning have taken place after very similar intervals between 17 and 20 days without cleaning. Nevertheless the impact of soiling varied strongly from +0.26 % to -2.77 % in DNI and from +0.16 % to -2.82 % in GHI. Since soiling cannot contribute to a higher measurement signal, positive impacts result from slightly unstable solar radiation conditions during the cleaning process that are larger than the soiling impact. Out of the four occurrences, only one shows a significant impact of soiling, which rises above the measurement uncertainty. This result confirms the lower sensitivity of the RSI sensor against soiling.

Table 7: Impact of soiling at 4 events of cleaning

Figure	days without cleaning	cleaning time	Soiling influence	DNI	GHI
a.	20	13:13	none	0.26%	-0.57%
b.	20	14:31	low	-0.54%	0.16%
c.	17	14:52	low	-0.35%	-0.8%
d.	18	8:45	significant	-2.77%	-2.82%

9.2. Observation of measurements during a period without cleaning

The following paragraph will focus on the sensitivity of RSI sensors compared to a pyrheliometer against soiling if no sensor cleaning is done during a period of one month. The readings of an uncleaned RSI and an uncleaned pyrheliometer were compared in May 2008 at the University of Almería. A cleaned set of pyranometers (one shaded, one unshaded) allowed for the calculation of a reference DNI. Furthermore, the soiling of pyranometers was analyzed at the PSA in late summer of 2005. The accuracy of daily irradiation measurements from pyranometers is stated by the manufacturer to range between ±2 %. This must be taken into consideration when evaluating the results.

The relative error of RSI and pyrheliometer with respect to the pyranometer reference DNI is plotted in the right graph of Figure 36 for the complete period of observation. It is clearly visible that the relative error caused by soiling of the uncleaned pyrheliometer almost follows a linear curve leading to roughly -25 % error after 31 days without cleaning. Meanwhile, the RSI measurement of DNI varies arbitrary in the range of ±2 %, which lies within the reference uncertainty. There is no continuous rise in the relative RSI error visible. The relative error changes between positive and negative values and meets zero even after 25 days without cleaning.

The results of another study about the pyrheliometer's sensitivity against soiling is shown in the left graph of Figure 36. In this case the reference is based on an uncleaned set of pyranometers. Since pyranometers are principally far less sensitive against soiling, the analysis can still serve as a fairly accurate source. The results of soiling impact shows almost the same behavior as the analysis of 2008, even though it origins from a different season and location. Also during this period, the pyrheliometer's readings suffer growing errors on a roughly linear curve, reaching its maximum after 31 days with about 31 % of relative error. The two studies certify the experiences made with the pyrheliometers that soiling influence of these sensors especially in summer times can be quite high, much higher than the accuracy of the pyrheliometers or the RSI sensors whereas the soiling influence of the RSI sensors is mostly below the measurement accuracy. Further results on soiling of RSIs are documented in [Geuder, 2006].

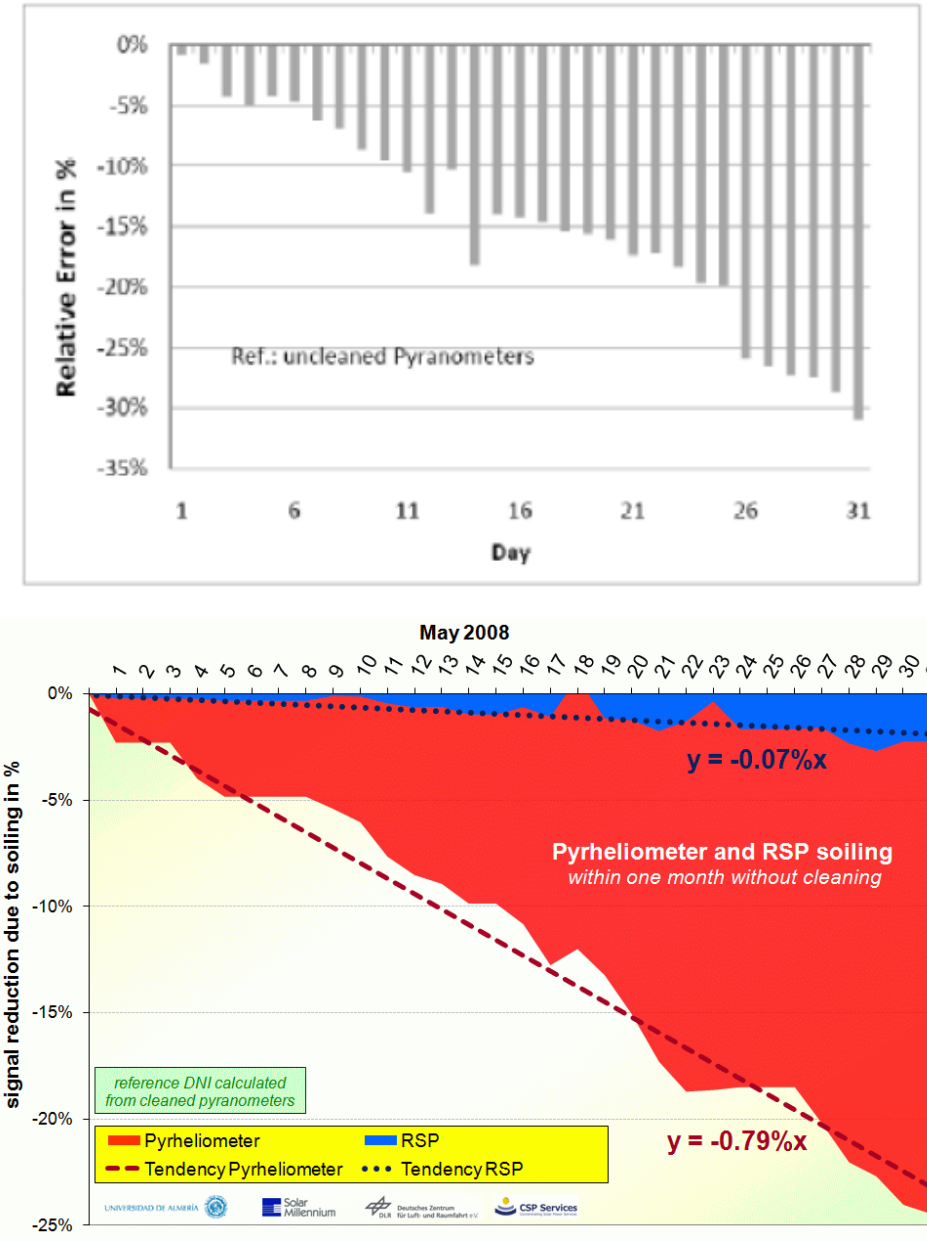

Figure 36: Relative error in DNI of uncleaned pyrheliometer with reference to cleaned pyranometers on PSA August 2005 (upper figure) and additional measurements by an uncleaned RSI at University of Almería in May 2008 (lower figure)

Concluding it can be stated that RSIs have a significant advantage against their high precision competitors, the tracked pyrheliometers if cleaning cannot be guaranteed on a daily basis.

10. Conclusion and Outlook

RSIs have proven to be appropriate instruments for diligent solar resource assessments for large-scale solar plant projects. This holds also and especially for concentrating solar technologies where the focus of the resource assessment lies on direct beam irradiation.

As for all meteorological sensors best practices must be followed to allow for utmost data quality. Well defined procedures must be followed for

- the selection of location for measurement station
- installation, operation and maintenance of measurement station, including the case of remote sites
- the documentation and quality control of the measurements
- and the correction of systematic errors & instrument calibration (procedure and frequency)

as presented in this document. Due to their lower maintenance requirements, lower soiling susceptibility, lower power demand, and comparatively lower cost, RSI show significant advantages over thermopile sensors when operated under the measurement conditions of remote weather stations. The initially lower accuracy of RSIs, which can yield deviations of 5 to 10 % and more, can be notably improved with proper calibration of the sensors and corrections of the systematic deviations of its response. Uncertainties of below 3 % for 10 min DNI averages and below 2 % for yearly DNI sums have been found in the various studies published so far.

Different RSI calibration methods exist and have been compared. Application of two or more calibration factors for the different irradiance components respectively yields noticeable higher accuracy than the application of only one calibration factor derived from GHI measurements.

The so far achieved measurement accuracy of RSIs can still be improved. The analysis of the transferability of correction and calibration between different climate zones, sites and altitudes will be continued. Further investigation of spectral and site dependent corrections is continued.

Acknowledgements

The comments and suggestions from IEA SHC task 46 members are highly appreciated. We thank the German Federal Ministry for Economic Affairs and Energy for the financial support within the INS project 1268 (Gefördert durch Bundesministerium für Wirtschaft und Energie aufgrund eines Beschlusses des Deutschen Bundestages). We thank Chris Kern for providing information concerning the RSR2.

References

[Alados1995] L. Alados-Arboledas, F. J. Batlles, F. J. Olmo, Solar Radiation Resource Assessment by Means of Silicon Cells, Solar Energy, Vol. 54 No. 3, 183-191 (1995).

[Augustyn2004] Augustyn, J., Geer, T., Stoffel, T., Kessler, R., Kern, E., Little, R., Vignola, F., Boyson, B., "Update of Algorithm to Correct Direct Normal Irradiance Measurements Made with a Rotating Shadow Band Pyranometer", Proc. Solar 2004, American Solar Energy Society, (2004)

[Augustyn2002] Augustyn, J., Geer, T., Stoffel, T., Kessler, R., Kern, E., Little, R., Vignola, F., "Improving the Accuracy of Low Cost Measurement of Direct Normal Solar Irradiance", Proc. Solar 2002, American Solar Energy Society, (2002)

[Batlles1995] F. J. Batlles, F. J. Olmo and L. Alandos-Arboledas: On Shadowband Correction Methods for Diffuse Irradiance Measurements, Solar Energy, Vol. 54 No. 2, 105-114 (1995)

[Biggs2000] LI-COR, Inc. (William W. Biggs), "PRINCIPLES OF RADIATION MEASUREMENT", Lincoln, Nebraska, USA

[Bird1984] Bird, R.E., A simple, solar spectral model for direct-normal and diffuse horizontal irradiance. Solar Energy, 1984. **32**(4): p. 461-471.

[Espinar2011] Espinar, B.; Wald, L.; Blanc, P.; Hoyer-Klick, C.; Schroedter-Homscheidt, M. & Wanderer, T. Report on the harmonization and qualification of meteorological data Project ENDORSE, Energy Downstream Service Providing Energy Components for GMES, Grant Agreement No. 262892, 2011. Available at http://www.endorse-fp7.eu/public_deliverables

[Geuder2003] Geuder, N., Ortmanns, W., Quaschning, V., Trieb, F., Schillings, C., Meyer, R., "Determination of Irradiation Data for Solar Based Energy Generation",ISES Solar World Congress,2003 June 14-19, Göteborg, Sweden, (2003).

[Geuder, 2006] Geuder, N., Quaschning, V., "Soling of Irradiation Sensors and Methods for Soiling Correction", Solar Energy 80, 1402-1409 (2006).

[Geuder2008] N. Geuder, B. Pulvermueller, O. Vorbrugg, Corrections for Rotating Shadowband Pyranometers for Solar Resource Assessment, Solar Energy + Applications, part of SPIE Optics + Photonics 2008, 10-14 August 2008, San Diego, USA (2008).

[Geuder2010] N. Geuder, R. Affolter, O. Goebel, B. Dahleh, M. Al Khawaja, S. Wilbert, B. Pape, B. Pulvermueller, Validation of Direct Beam Irradiance Measurements from Rotating Shadowband Pyranometers in a Different Climate, Proceedings of SolarPACES Conference, Perpignan (2010).

[Geuder2014] Geuder, N., F. Wolfertstetter, S. Wilbert, D. Schueler, R. Affolter, E. Luepfert, and B. Espinar. "Screening and Flagging of Solar Irradiation and Ancillary Meteorological Data." In International Conference on Concentrating Solar Power and Chemical Energy Systems, SolarPACES 2014. Beijing, China, 2014.

[Gueymard2001] Gueymard, C. A. "Parameterized transmittance model for direct beam and circumsolar spectral irradiance." Solar Energy **71**(5): 325-346 (2001).

[Holben1998] Holben, B., T. Eck, et al. "AERONET--A federated instrument network and data archive for aerosol characterization." Remote Sensing of Environment **66**(1): 1-16 (1998).

[ISO9059 1990] ISO 9059:1990(E), Solar energy – Calibration of field pyrheliometers by comparison to a reference pyrheliometer, International Organization for Standardization, Case Postale 56, 1211 Genève, Switzerland (1990).

[ISO9847 1992] ISO 9847:1992(E), Solar energy – Calibration of field pyranometers by comparison to a reference pyranometer, International Organization for Standardization, Case Postale 56, 1211 Genève, Switzerland (1992).

[ISO9846 1993] ISO 9846:1993, Solar energy – Calibration of a pyranometer using a, International Organization for Standardization, Case Postale 56, 1211 Genève, Switzerland (1993).

[Journee2011] Journée, M. Bertrand, C. Quality control of solar radiation data within the RMIB solar measurements network. Solar Energy 85 (2011), 72-86.

[King1997] D. L. King, D. R. Myers, Silicon Photodiode Pyranometers: Operational Characteristics, Historical Experiences, and New Calibration Procedures, 26th IEEE Photovoltaic Specialists Conference, (1997).

[King1997b] King, D.L., W.E. Boyson, and B.R. Hansen. "Improved Accuracy for Low-Cost Solar Irradiance Sensors." PBD: [1997], Medium: ED; Size: 4 p., OSTI ID: 661542; Legacy ID: DE98002961. http://www.osti.gov/scitech//servlets/purl/661542-B0ZFIq/webviewable/. 1997..

[King1998] King, D. L., Boyson, W. E., Hansen, B. R., and Bower, W. I., 1998, "Improved Accuracy for Low-Cost Solar Irradiance Sensors," 2nd World Conference and Exhibition on Photovoltaic Solar Energy Conversion Proceedings; July 6–10, 1998, Vienna, Austria.

[Kern2010] Edward C. Kern, J., Calibration Methods for Silicon Photodiode Pyranometers used in Rotating Shadowband Radiometers, in Proceedings of SolarPACES Conference, Perpignan (2010).

[LICOR2005] LI-COR® Biosciences, LI-COR Terrestrial Radiation Sensors – Instruction Manual, LI-COR, Inc., Lincoln, Nebraska 68504, USA (2005).

[Long2002] Long, C.N., Dutton, E.G.. Baseline Surface Radiation Network (BSRN) Global Network recommended QC tests, V2.0. http://epic.awi.de/30083/1/BSRN_recommended_QC_tests_V2.pdf, 2002 (last accessed 2014-09-25).

[Maxwell1993] Maxwell, E., Wilcox, S. and Rymes, M. Users Manual for SERI QC Software. Assessing the Quality of Solar radiation Data. Technical report NREL TP-463-5608 DE93018210. 1993. Available at http://www.nrel.gov/docs/legosti/old/5608.pdf (last accessed 2014-09-26).

[Michalsky1988] Michalsky, J. J., "The Astronomical Almanac's Algorithm for Approximate Solar Position (1950-2050)", Solar Energy Vol. 40, No. 3, 227-235 (1988).

[Myers2011] Myers, D., Quantitative Analysis of Spectral Impacts on Silicon Photodiode Radiometers. presented at SOLAR 2011, May 17–21, 2011. Raleigh, North Carolina (2011).

[NREL2003] Under NREL subcontract: J. Augustyn, J. Big, R. Little, F. Vignola, "FINAL REPORT ON RESEARCH PROJECT TO REDUCE THE COST OF ACCURATE AND RELIABLE GROUND STATION MEASUREMENT OF DIRECT BEAM SOLAR IRRADIANCE", September 2003

[Pape2009] B. Pape, J. Battles, N. Geuder, R. Zurita, F. Adan, B. Pulvermueller, Soiling Impact and Correction Formulas in Solar Measurements for CSP Projects, Proceedings of SolarPACES Conference, Berlin (2009).

[Stoffel2010] Stoffel, T., Renne, D., Myers, D., Wilcox, S., Sengupta, M., George, R., and Turchi, C., 2010, "Concentrating Solar Power: Best Practices Handbook for the Collection and Use of Solar Resource Data (CSP)," National Renewable Energy Laboratory (NREL), Golden, CO.

[Vignola1999] Vignola, F., "Solar Cell Based Pyranometers: Evaluation of Diffuse Responsivity", Proceedings of the 1999 Annual Conference American Solar Energy Society, June 1999, (1999).

[Vignola2009] F., "Solar cell based pyranometers: evaluation of the diffuse response," Proc. PROCEEDINGS OF THE SOLAR CONFERENCE, AMERICAN SOLAR ENERGY SOCIETY; AMERICAN INSTITUTE OF ARCHITECTS, pp. 255-260.

[Vignola2006] F. Vignola, Removing Systematic Errors from Rotating Shadowband Pyranometer Data, Solar 2006, American Solar Energy Society, 7th – 13th of July 2006, Denver, Colorado, USA, (2006).

[Dubis2014] M. Dubuis, M. Hauser, C. Félix, B. Calpini and L. Vuilleumier Performance Evaluation of Radiation Sensors for the Solar Energy Sector Presented at the 13th BSRN Scientific Review and Workshop, Bologna, 9-12 September 2014.

[Wilcox2011] Wilcox, S. Cormack, P. Implementing Best Practices for Data Quality Assessment of the National Renewable Energy Laboratory's Solar Resource and Meteorological Assessment Project. SOLAR 2011, Raleigh, North Carolina, May 16-21, 2011.

[WMO2008] WMO, 2008, "Guide to Meteorological Instruments and Methods of Observation, WMO-No. 8, Seventh edition."

[Young 1994] Young, A. T., "Air Mass and Refraction", Applied Optics Vol. 33 No. 6, (1994).